

Review

Research Progress on Thin-Walled Sound Insulation Metamaterial Structures

Yumei Zhang¹, Jie Zhang² , Ye Li³ , Dan Yao¹, Yue Zhao^{1,*}, Yi Ai¹, Weijun Pan¹ and Jiang Li²

¹ College of Air Traffic Management, Civil Aviation Flight University of China, Guanghan 618307, China; wjpan@cafuc.edu.cn (W.P.)

² State Key Laboratory of Polymer Materials Engineering/Polymer Research Institute, Sichuan University, Chengdu 610065, China; jzhang2019@scu.edu.cn (J.Z.); li_jiang@scu.edu.cn (J.L.)

³ School of Automotive and Traffic Engineering, Jiangsu University of Technology, Changzhou 213164, China

* Correspondence: zhaoyue@cafuc.edu.cn

Abstract: Acoustic metamaterials (AMs) composed of periodic artificial structures have extraordinary sound wave manipulation capabilities compared with traditional acoustic materials, and they have attracted widespread research attention. The sound insulation performance of thin-walled structures commonly used in engineering applications with restricted space, for example, vehicles' body structures, and the latest studies on the sound insulation of thin-walled metamaterial structures, are comprehensively discussed in this paper. First, the definition and math law of sound insulation are introduced, alongside the primary methods of sound insulation testing of specimens. Secondly, the main sound insulation acoustic metamaterial structures are summarized and classified, including membrane-type, plate-type, and smart-material-type sound insulation metamaterials, boundaries, and temperature effects, as well as the sound insulation research on composite structures combined with metamaterial structures. Finally, the research status, challenges, and trends of sound insulation metamaterial structures are summarized. It was found that combining the advantages of metamaterial and various composite panel structures with optimization methods considering lightweight and proper wide frequency band single evaluator has the potential to improve the sound insulation performance of composite metamaterials in the full frequency range. Relative review results provide a comprehensive reference for the sound insulation metamaterial design and application.

Keywords: metamaterial; sound insulation; composite structure; light weight; optimization



Citation: Zhang, Y.; Zhang, J.; Li, Y.; Yao, D.; Zhao, Y.; Ai, Y.; Pan, W.; Li, J. Research Progress on Thin-Walled Sound Insulation Metamaterial Structures. *Acoustics* **2024**, *6*, 298–330. <https://doi.org/10.3390/acoustics6020016>

Academic Editors: Heow Pueh Lee and Jian Kang

Received: 31 December 2023

Revised: 15 March 2024

Accepted: 22 March 2024

Published: 26 March 2024



Copyright: © 2024 by the authors. Licensee MDPI, Basel, Switzerland. This article is an open access article distributed under the terms and conditions of the Creative Commons Attribution (CC BY) license (<https://creativecommons.org/licenses/by/4.0/>).

1. Introduction

In recent decades, AMs have received widespread attention, and significant progress has been made in their development, with notable breakthroughs achieved in the arbitrary manipulation and control of the refraction, reflection, and absorption of sound waves [1]. Metamaterials are artificial periodic structures with extraordinary physical properties that natural materials do not have. Veselago first proposed the concept of metamaterials in 1968 [2]. Since then, many different branches of metamaterials have developed, such as electromagnetic and optical metamaterials [3–6]. Acoustic metamaterials (AMs) are an important branch of metamaterials. Sialas et al. proposed the concept of phononic crystals in 1992 [7]. In the early stage of their research, the main focus was on the generation mechanism and modulation of the band gap [8,9]. In 2000, Liu et al. [10,11] found that the local resonance structure has a negative mass density, which can improve the sound absorption effect of the structure in the low-frequency band. Recently, Ciaburro et al. studied the sound absorption properties of metamaterials composed of cork sheets, thumbtacks, and buttons, and the sound absorption coefficient of the three-layer metamaterial was predicted by an artificial neural network model [12,13]. In addition to sound absorption, research on acoustic metamaterials has also included directional propagation of sound waves [14],

conversion of cylindrical waves to plane waves [15], acoustic focusing [16], and acoustic stealth [17].

Many reviews related to acoustic metamaterials have been undertaken [1,18–31]. Liao et al. introduced phononic crystals and related theories with a focus on additive manufacturing [1]. Cummer et al. outlined the designs and properties of metamaterial parameters (for example, negative refractive index) [18]. Chen et al. highlighted the tunable acoustic metamaterials and corresponding modulation techniques [20]. Ji et al. introduced the classification and application of piezoelectric acoustic metamaterials from the perspective of passive and active acoustic metamaterials [26]. Ma et al. considered the aspects of sound absorption, sound insulation, and noise reduction of metamaterials [21]. Yin et al. systematically reviewed the function of phononic crystals [28,31]. Among the applications of AMs in different fields, panels are one of the most important body structures of transportation vehicles [32–35], and acoustic metamaterials aimed at improving sound insulation properties have also been widely developed. However, there has been a lack of a comprehensive and in-depth review of these materials in the literature.

Sound insulation is a way to reduce the airborne sound from the propagation path. The acoustic environment in the cabin (car) has the thorny problem of significant mid- and low-frequency noise [36–39]. Traditional sound insulation structures obey mass law and have small sound insulation at low frequencies. The emergence of AMs provides new ideas for mid- and low-frequency noise control. At the same time, due to the complex structural design, limited band gaps, and added mass of AM sound insulation structures, there are challenges in the manufacturing, frequency band broadening, and engineering applications of AMs. The goal of this article was to comprehensively analyze the structural characteristics, research theories, and challenges of these materials by summarizing the latest progress in metamaterial sound insulation panel structures.

The structure of this article is as follows: Section 2 introduces the definitions of sound insulation quantity, modeling approaches of metamaterial STL and mass law, as well as the main methods of sound insulation test research; Section 3 provides a detailed classification and review of the research contents of four categories of sound insulation metamaterial panel structures and their optimization; Section 4 presents statistics on the fabrication approaches of STL test samples and discusses the challenges; finally, Section 5 summarizes the status and challenges of metamaterial sound insulation panel research and looks at possible future research directions.

2. Materials and Methods

The definition of STL, modeling approach of metamaterials STL, mass law, and STL measurement are introduced.

2.1. Definition of Sound Transmission Loss

Sound insulation is the use of materials or structures to hinder the spread of noise. The amount of sound insulation is the strength of the sound insulation capability and is a function of the transmission coefficient. The expressions of the transmission coefficient τ and the sound transmission loss (STL) are as follows [40,41]:

$$\tau = \frac{E_t}{E_i}, \quad (1)$$

$$\text{STL} = 10\lg\left(\frac{1}{\tau}\right), \quad (2)$$

where E_i is the incident sound energy and E_t is the transmitted sound energy.

2.2. Modeling Approaches of Metamaterials STL

The above formula defines the transmission coefficient and the STL. From a prediction perspective, the incident and transmitted sound energy need to be solved. According to the STL frequency and the complexity of the structure, traditional panel structures gener-

ally use the impedance method [42], transfer matrix method [43], and wave propagation method [44] as analytical methods and use numerical methods such as the finite element method (FEM), boundary element method (BEM), statistical energy analysis (SEA) [45], and their hybrid methods, namely, Wave-SEA [46], FE-SEA [47], and Wave-FEM [48]. There are many classic books [40,41,49,50] and reviews on these methods [23,51]. Theoretical methods related to the band gap and the response of acoustic metamaterials mainly include acoustic wave [1], crystal lattice [52,53], energy band theory [54], effective medium theory, and general Snell's law [55,56].

Three methods are introduced here as examples to illustrate the STL modeling approaches of metamaterial structures, namely, plane wave expansion (PWE) method, effective medium method, and FEM.

2.2.1. PWE

In uniform plates with periodic supports or stiffeners, the PWE method is commonly used. It was extended to the STL analysis by Xiao et al [57]. The governing equation for the locally resonant plate is given in Equation (3). Since the displacement $w(\mathbf{r})$, sound pressure p , etc., are summation terms of reciprocal-lattice vector \mathbf{G} , the control equation can be written in matrix form in Equation (4); then, the coefficients vector $\mathbf{W}_{\mathbf{G}}$ can be solved.

$$D\nabla^4 w(\mathbf{r}) - \rho h \omega^2 w(\mathbf{r}) = p_{\text{inc}}(\mathbf{r}, z)_{z=0} + p_{\text{ref}}(\mathbf{r}, z)_{z=0} - p_{\text{tr}}(\mathbf{r}, z)_{z=0} + \sum_{j=1}^N \sum_{\mathbf{R}} f_j(\mathbf{r}_j + \mathbf{R}) \delta[\mathbf{r} - (\mathbf{r}_j + \mathbf{R})] \quad (3)$$

$$\left([\mathbf{K}_p] + i\omega[\mathbf{C}_f] - \omega^2[\mathbf{M}_p] + [\mathbf{D}_r] \right) \{\mathbf{W}_{\mathbf{G}}\} = 2P_0 S \{\delta_{0-\mathbf{G}}\}, \quad (4)$$

where $w(\mathbf{r})$ is the transverse displacement of the plate, p_{inc} , p_{ref} , and p_{tr} are the incident, reflected, and transmitted sound pressure, D is the plate bending stiffness, $f_j(\mathbf{r}_j + \mathbf{R})$ refers to the force applied to the plate by the resonator, \mathbf{K}_p and \mathbf{M}_p are plate stiffness and mass matrices, \mathbf{C}_f is the fluid loading matrix, and \mathbf{D}_r is the dynamic stiffness matrix of the resonators, the details expression of which can be seen in reference [57].

The PWE can be used to solve the displacement and STL of finite locally resonant metamaterials through the modal superposition method [58]. The fast plane wave expansion (FPWE) approach can also be used to determine the band diagram effectively [59].

2.2.2. Effective Medium Method

When the cell sizes are much smaller than the wavelength of the bending waves in the matrix plate, the locally resonant plate metamaterial can be simplified to an isotropic homogeneous plate structure with equivalent dynamic mass density ρ_{eff} [57]. Then, the governing equation of the locally resonant plate under acoustic wave excitation can be expressed as follows:

$$D\nabla^4 w(\mathbf{r}) - \rho_{\text{eff}} h \omega^2 w(\mathbf{r}) = p_{\text{inc}}(\mathbf{r}, z)_{z=0} + p_{\text{ref}}(\mathbf{r}, z)_{z=0} - p_{\text{tr}}(\mathbf{r}, z)_{z=0}. \quad (5)$$

2.2.3. FEM

To validate the theoretical model or predict the STL of sound insulation metamaterials, the numerical FEM method is usually used, and most of the time, the commercial software COMSOL is chosen. Figure 1 gives the FEM model or illustration of the normal incidence STL prediction of different metamaterial unit cells [60–63]. The normal incidence excitation is applied, and the finite element models of sound insulation components, incident, and reflected acoustic fields are built. Two ends of the model are set to sound absorption boundaries, non-reflective boundaries, or perfectly matched layers (PML). Since metamaterials are periodic, corresponding periodic boundary conditions can be set to simulate the large-size structure.

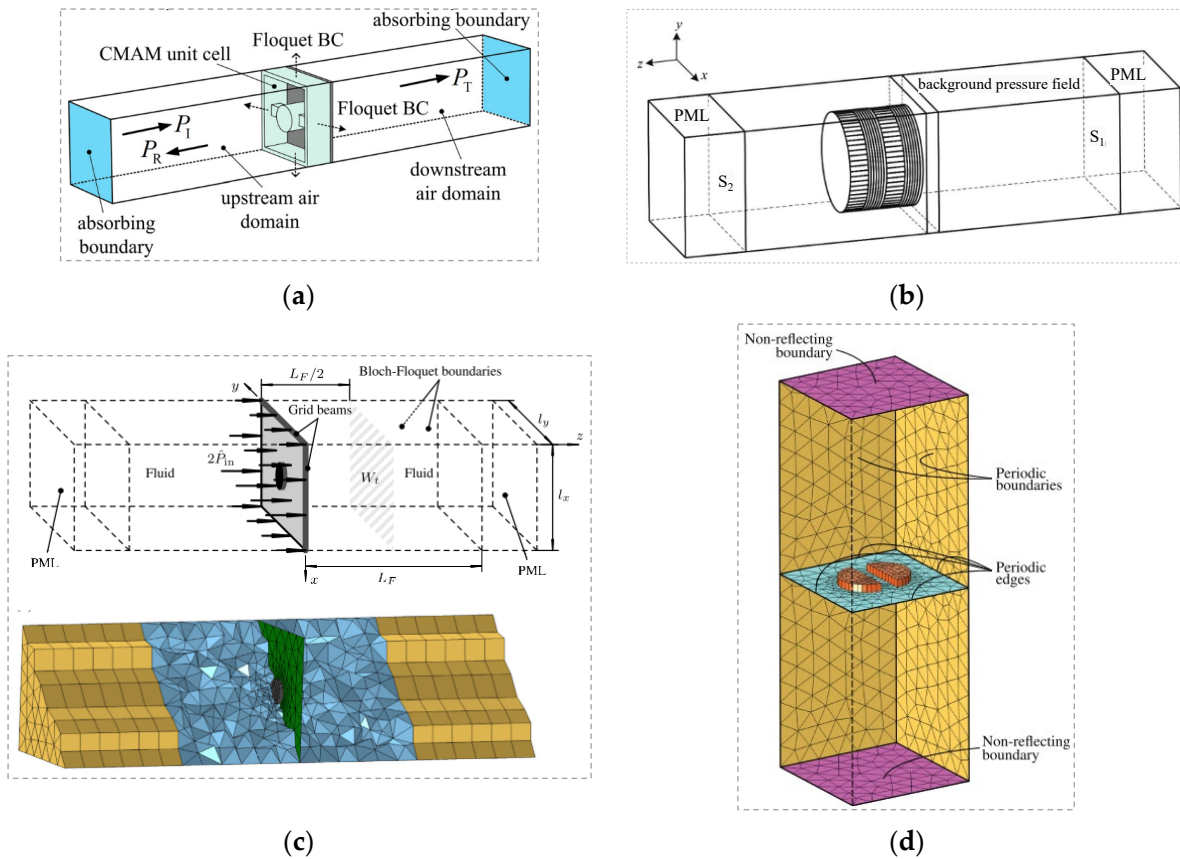


Figure 1. The FEM model or illustration of the normal incidence STL of the unit cell: (a) constrained membrane acoustic metamaterial (CMAM) sample, reproduced from [60]; (b) single-layer perforated plate acoustic metamaterial (PAM), reproduced from [61]; (c) PAM with elastic unit cell edges, reproduced from [62]; and (d) multiple masses per unit cell PAM, reproduced from [63].

2.3. Mass Law

Rayleigh proposed the sound insulation theory of incompressible infinite walls in 1896 and obtained the “mass law” of thin plate sound insulation [28,64]; that is, the STL under normal incidence of sound waves can be approximately expressed as follows:

$$STL = 10 \lg \left[1 + \left(\frac{\omega \rho h}{2 \rho_0 c_0} \right)^2 \right], \tag{6}$$

where ω is the angular frequency, and ρ and h are the density and thickness of the material, respectively. ρ_0 and c_0 are the density and speed of sound of the fluid medium. In Equation (6), if the surface density of the material is doubled, the STL will have an increment of 6 dB, which is the mass law of thin plate sound insulation.

The mass law cannot reflect the boundary condition, natural frequency, and coincident frequency of finite structures, but it is still one of the most widely used principles and references for sound insulation research and engineering applications. The mass law shows that to improve the sound insulation performance of a homogeneous plate structure, it is necessary to increase the material thickness or density, which is contrary to the development trend of lightweight structural design. Therefore, achieving efficient sound insulation of lightweight structures is a key issue in the field of engineering [28].

2.4. Measurement of Sound Insulation

In addition to simulation and theoretical prediction, sound insulation measurement is one of the main research methods for model validation and verification before proceeding

to engineering applications [65,66]. For small specimens, with the development of 3D printing technology [67], impedance tubes are mainly used to test normal sound insulation (the diameter of medium- and low-frequency sound insulation test specimens is generally 100 mm), as shown in Figure 2 [68]. To test the reverberation sound insulation, an acoustic chamber is usually used, such as a reverberation-reverberation chamber, reverberation-anechoic chamber, etc., which is based on the sound intensity method or sound pressure method [69,70]. Yao et al. included photographs of a sound insulation capacity test with a specimen size of about 1 m*1 m between two reverberation chambers, as shown in Figure 3 [71].

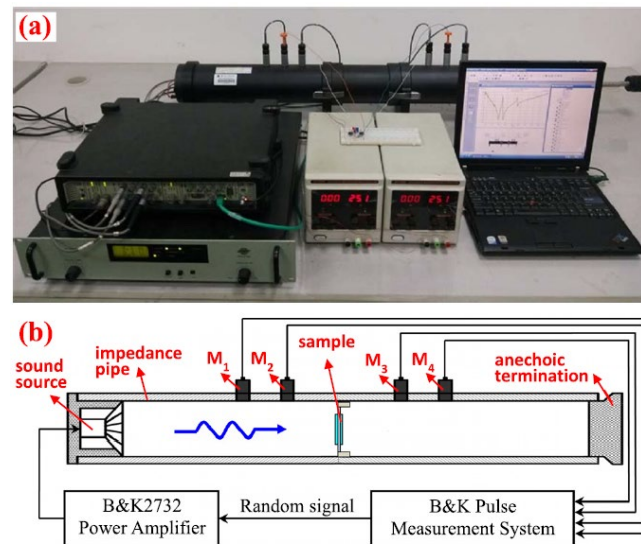


Figure 2. Illustration of STL measurement through impedance tube, reproduced from [68]. (a) Photo of the measurement set-up. (b) Sketch of the measurement set-up.

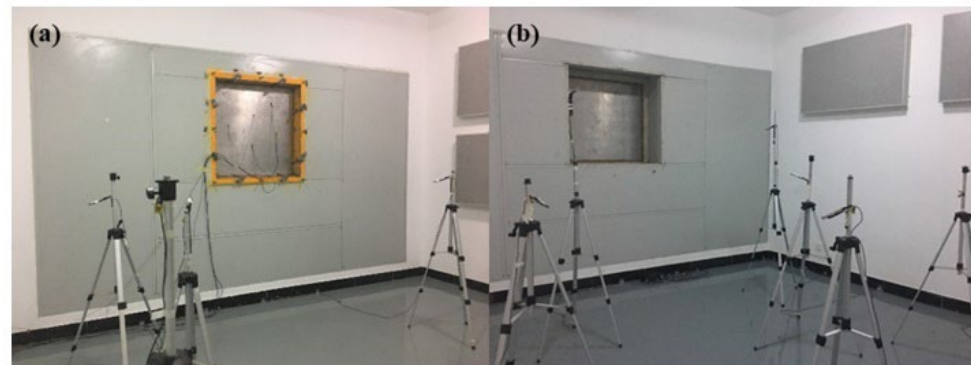


Figure 3. Illustration of STL measurement through acoustic room, reproduced from [71]. (a) Panel installation status on the side of source room, and (b) Panel installation status on the side of receiving room.

In addition to plane and reverberation sound insulation, the frequency bands concerned with sound insulation depend on the specific application scenario. Usually, the frequency band is wide, although it does not cover the audible range of the human ear. The highest frequency can reach 6000 Hz and above. Therefore, the evaluation indicators of sound insulation usually include the frequency STL and some single-value evaluation indicators [72], such as the average STL [58,73,74], weighted STL R_w , etc [75].

3. Results

This section gives the review results of sound insulation metamaterial structures studies in recent years and divides them into four categories according to different structural characteristics, namely, the membrane-type, plate-type, and smart-material-type sound insulation metamaterials, and composites combined with metamaterials. Here, we describe the structural characteristics, research methods, tests, results, etc.

3.1. Membrane-Type Sound Insulation Metamaterial

Membrane-type structures are an important type of AM that consists of a membrane fixed on a hard boundary and a central mass block [1]. A classic membrane-type metamaterial usually consists of the membrane, boundary, and central mass. This section introduces the existing research on membrane-type sound insulation metamaterials from the perspectives of classic and complex structures, new material membrane-type metamaterials, multi-frequency membrane-type metamaterials, and membrane-type metamaterial structure optimization.

3.1.1. Classic Membrane-Type Metamaterial

Hashimoto et al. (1991) [76], conducted early research on the sound insulation theory and actual measurement of classic membrane-type metamaterials. They provided an analytical model for calculating the sound insulation of membrane-type phononic crystals based on the modal superposition method, based on analyzing the vibration modal shape change of the membrane after adding a mass block. The sound insulation was measured for a 10 cm × 15 cm × 0.3 mm sample in a semi-anechoic chamber. The results showed that the amount of low-frequency sound insulation can be effectively increased by adjusting the concentrated mass and cell size [76]. Ho et al. further compared the sound insulation effect of the membrane-type metamaterial shown in Figure 4a with the mass law and tested the resonant unit, made of metal balls and silicone rubber, through an impedance tube. The research results confirmed that an area mass of almost the same density of locally resonant sonic material samples can break the mass law [77]. Yang et al. calculated the effective dynamic mass of the membrane structure through finite element simulation and analyzed the sound transmission mechanism at the peak frequency of sound insulation [78]. Naify et al. considered the influence of membrane tension. As shown in Figure 4b, the measurement results of the impedance tube were compared with the results of the coupled field acoustic-structural finite element. The results showed that the peak frequency can be adjusted through the membrane mass size and membrane tension. At the same time, membrane-type acoustic metamaterial with a negative dynamic mass density increases the STL of the specific mass law by five times at the low-frequency narrow-band peak frequency (100 Hz) [79]. When Zhang et al. predicted the sound insulation of membrane-type acoustic metamaterials based on the modal superposition method, they found that the first resonance frequency and STL peak frequency strongly depend on the additional mass, while the second resonance frequency is mainly affected by the membrane characteristics [80]. Based on the research on single-cell and finite-size membrane-type metamaterials, Varanasi et al. considered the influence of size. As shown in Figure 4c, the infinite plate was realized through the periodic boundary conditions of a single cell. Finite element simulation and sound insulation test research on impedance tubes with a single unit cell structure showed that better sound insulation results could be obtained by adjusting the unit cell length, geometry, and average area mass [81].

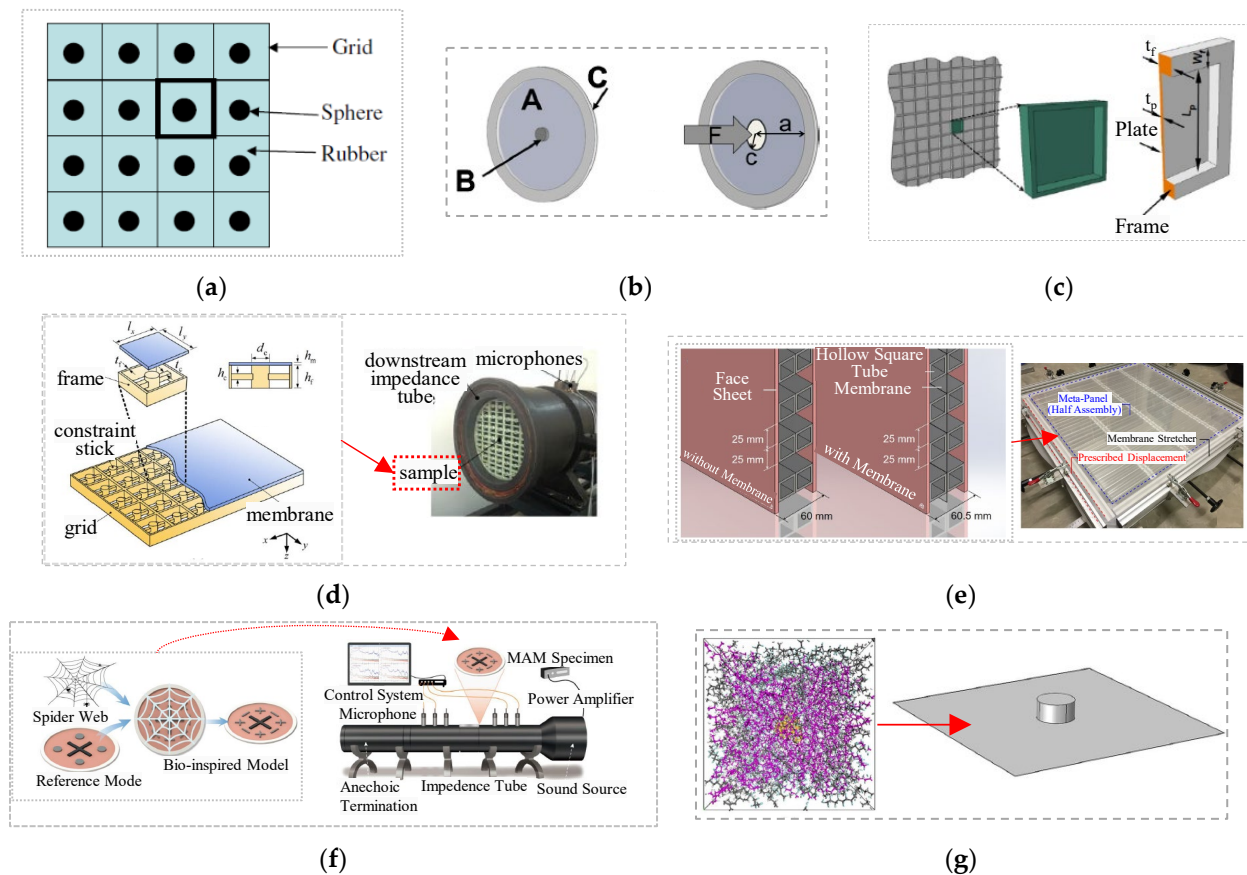


Figure 4. Classic and complex membrane-type metamaterial. (a) Schematics of the locally resonant metamaterial samples, reproduced from [77]. (b) Membrane-mass schematic with support ring, reproduced from [79]. (c) Cellular panel with its unit cell and a cutaway view, reproduced from [81]. (d) Unit cell of constrained membrane-type acoustic metamaterial and a photograph of the experimental setup for STL measurements, reproduced from [60]. (e) 3D representation of the meta-panel without (left) and with (right) the membrane and in-house designed membrane stretching mechanism, reproduced from [82]. (f) Bionic design and test equipment, reproduced from [83]. (g) Particle-enhanced ethylene propylene diene monomer/ethylene tetrafluoroethylene and membrane-type acoustic metamaterials structure of particle reinforced polymer, reproduced from [84].

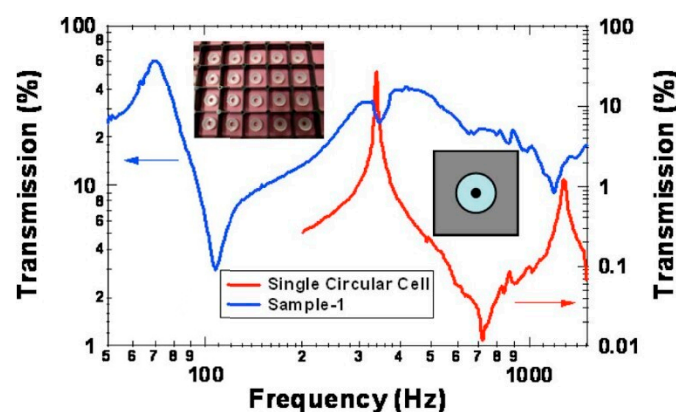
3.1.2. More Complex Membrane-Type Metamaterials

With the development of membrane-type metamaterial research, more complex structures and materials have emerged, such as constrained membrane acoustic metamaterials, flexible frame membrane structures, bionic membrane structures, and new material membrane structures. As shown in Figure 4d, a constrained membrane acoustic metamaterial (CMAM) has been proposed. An STL peak of 26 dB was achieved at 140 Hz. Three samples with the same geometry and materials but different constraints were manufactured, and their sound insulation was tested through an impedance tube, which demonstrated the tunability of the STL peak at low frequencies [60]. In a study of the vibration effects of large-size samples and frames, as shown in Figure 4e, Ang et al. proposed a large-size (0.8 m × 0.8 m) membrane-type acoustic metamaterial plate and conducted a reverberation-anechoic chamber experimental evaluation and FEM simulation. The results showed that the combined membrane was able to improve broadband STL, with an STL increase of up to 7.4 dB at 380 Hz. They also showed that the broadband sound insulation performance of the element panel was related not only to the membrane resonance but also to the frame structure vibration [82]. In a study of bionic complex membranes inspired by spider webs, a bionic spider web-type membrane acoustic metamaterial was designed by combining a

membrane, a frame, and a set of resonators, as shown in Figure 4f. Through finite element simulation and impedance tube experimental results, it was shown that the mass of the bionic model was reduced by 19%, and the bandwidth was expanded by 61% [83]. In terms of new materials, as shown in Figure 4g, Li et al. studied the acoustic transmission loss in particle-reinforced rubber-based membrane-type acoustic metamaterials [84]. Based on the discrete point matching method, the acoustic transmission loss characteristics were predicted. The results showed that this structure makes up for the low-frequency sound insulation defects of traditional membrane materials. STL of up to 60 dB can be achieved around 0.5 kHz, with superior results compared to the same mass membrane-type structures over the entire low-frequency range (50–1000 Hz).

3.1.3. Multi-Frequency Membrane-Type Metamaterials

Even though the research on membrane-type sound insulation metamaterial structures has led to the development of complex structures and advanced materials, scholars are still pursuing sound insulation structures with a wider frequency range. Multi-frequency membrane types have developed, such as simple superposition of membrane structures and membrane-type cells with multiple masses or shapes. For example, for a simple superposition of membrane structures, as shown in Figure 5a, Yang et al. studied the transmission spectrum of a stacked panel and showed that a broadband shield can be constructed by simply stacking several single membrane-type metamaterials with strategically chosen different frequencies regimes [85]. Multi-mass metamaterial cells with more complex shapes and arrangements are shown in Figure 5b. Naify et al. proposed a membrane-type acoustic metamaterial with a coaxial ring mass. By adjusting the number, center, and ring, the mass distribution between the masses and the radius of the ring can be used to adjust the sound insulation frequency band and peak value of the structure. The sound insulation results of finite element simulation and impedance tube testing showed that this was better than having only a central mass [86]. As shown in Figure 5c, it is also possible to embed metamaterials of different masses in adjacent cells. The sound insulation tested through an impedance tube showed that multiple sound insulation peaks can be obtained [87]. Research on the impact of mass eccentricity has also been carried out. As shown in Figure 5d, a membrane-type acoustic metamaterial (160 mm × 160 mm) with eccentric mass was studied based on finite element simulation and acoustic impedance tube testing. The results showed that by optimizing the eccentricity, the distribution of mass can improve the sound insulation performance [88].



(a)

Figure 5. Cont.

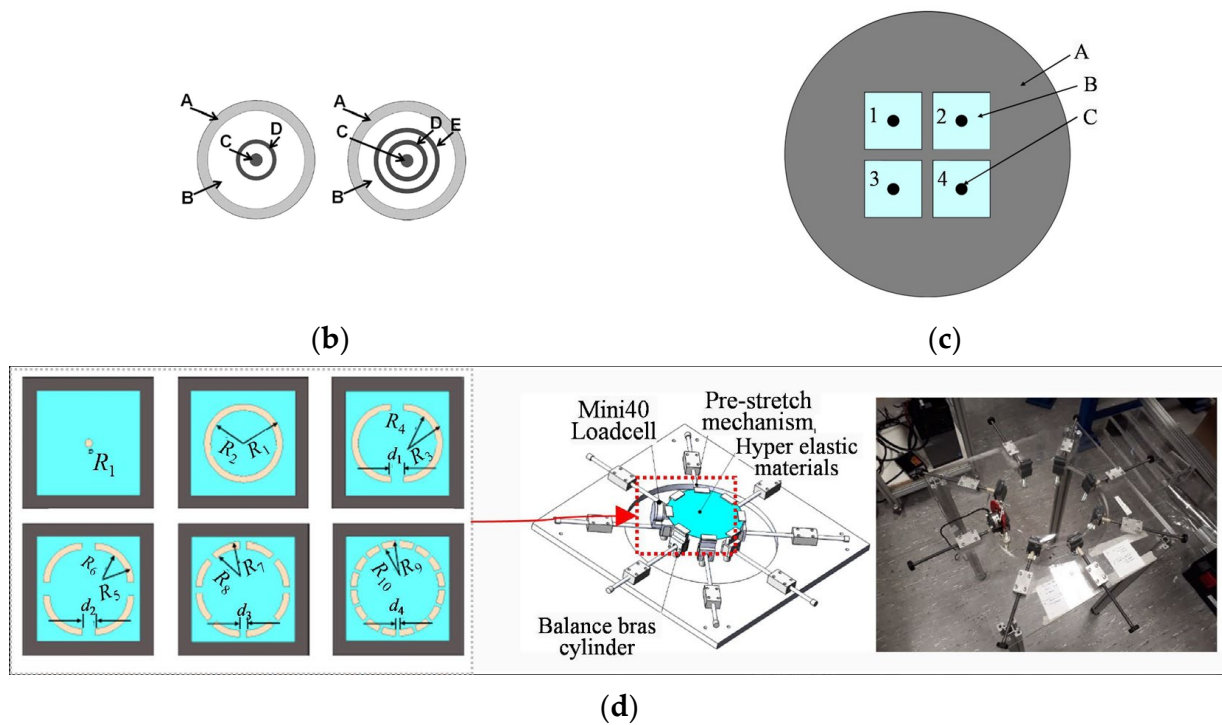


Figure 5. Multi-frequency membrane-type metamaterial. (a) Transmission spectra of a single circular cell (red curve) with an attached mass of 0.11 g and Sample-1 (blue curve) with an attached mass of 0.71 g, reproduced from [85]. (b) One ring mass and two ring masses: A, support structure; B, membrane; C, central mass; D, ring mass 1; E, ring mass 2, reproduced from [86]. (c) Schematic of the samples and the naming convention for the mass distribution of the four elements: A, support frame; B, membrane; C, attached mass, reproduced from [87]. (d) Various mass configurations on the membrane and producing the tensed membrane, reproduced from [88].

3.2. Plate-Type Sound Insulation Metamaterial

Plate-type metamaterials are realized by periodically arranging local resonance structures on the plate. The local resonance structure absorbs a large amount of energy due to resonance and reduces the vibration and sound radiation at the corresponding frequency of the substrate panel, thus achieving a sound insulation effect. The difference from membrane-type metamaterials is that there are frames between the membrane units.

3.2.1. Classical Local Resonance Plate-Type Metamaterial

A typical local resonance plate is a mass–spring system based on a simplified model. The actual structure is composed of cylinders of two materials, corresponding to the mass and spring structures of the local resonance structure, as shown in Figure 6a–c. Fokin et al. developed an inversion method to extract the resonators' effective properties from the reflection and transmission coefficients [54]. Among the innovations in theoretical methods, Xiao et al. developed a method based on the plane wave expansion method and effective medium method to study the reverberation sound insulation of plate-type metamaterials with the periodic addition of local resonators on thin plates. The structure is shown in Figure 6a. The results showed that at frequencies within the mass law region and the coincident region, metamaterial plates have much greater STL than bare plates (with the same surface mass density) [57]. As shown in Figure 6b, Xiao et al. further developed a semi-analytical calculation method based on the dynamic effective surface mass density for periodic mass block array thin plate metamaterials, and the theoretical method was verified by testing a specimen with a size of 840 mm × 840 mm in a semi-anechoic chamber. The results showed that these types of plate-like superstructures exhibit significantly increased STL in the low-frequency range compared to mass law values [89]. In a study considering

the production process, as shown in Figure 6c, Nakayama et al. proposed a local working metamaterial sound insulation structure that is easy to mass-produce. The sound insulation performance of the structure was predicted through the finite element method, and the sound pressure outside the sound insulation enclosure with and without the metamaterial structure was compared through tests under a 630–1250 Hz sound source, confirming the superior sound insulation performance of the metamaterial structure [90].

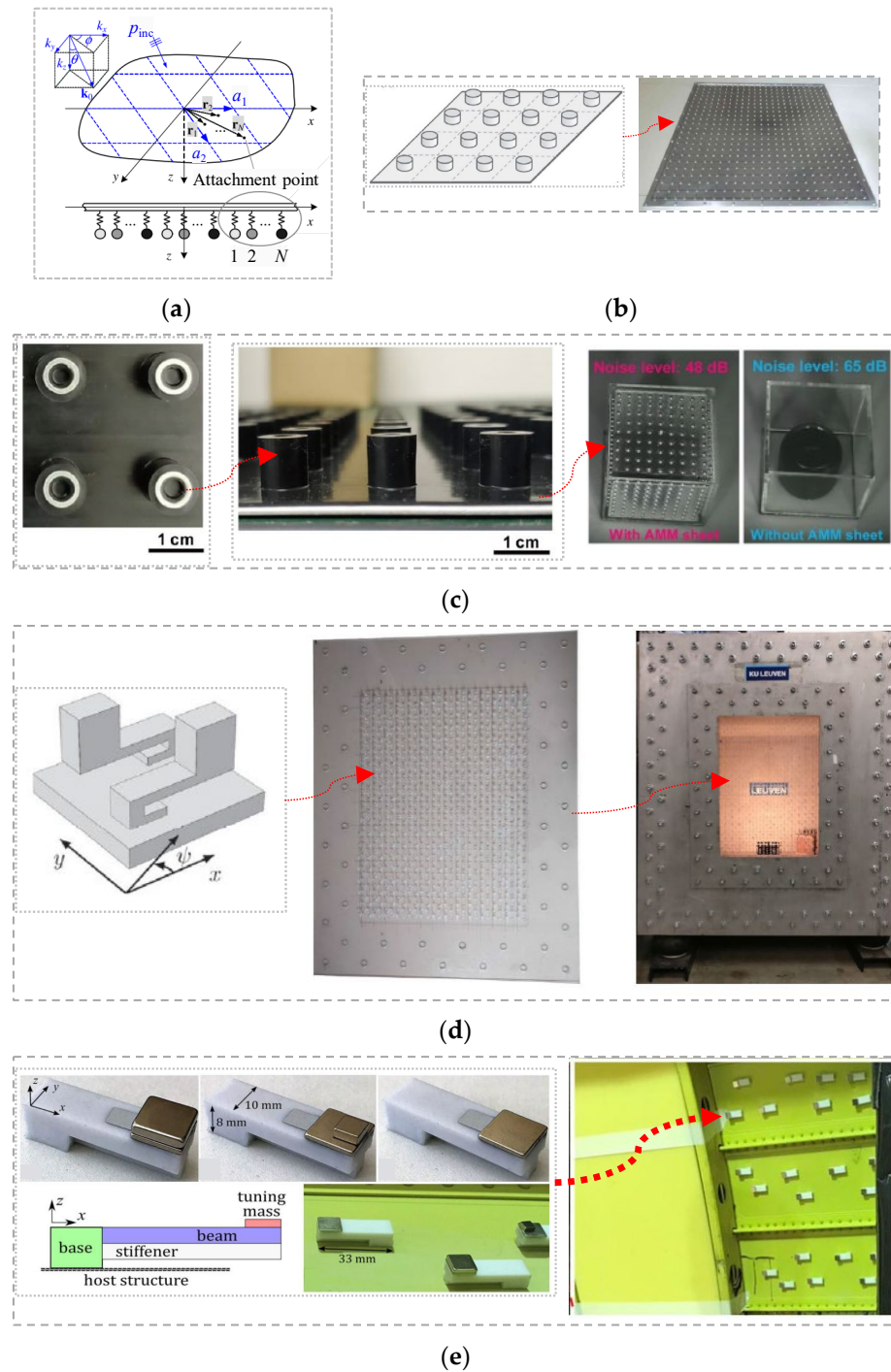


Figure 6. Classical and cantilever beam-type local resonance plate-type metamaterial. (a) Schematic diagram of an infinite locally resonant thin plate with 2D multiple periodic arrays of attached spring-mass resonators, reproduced from [57]. (b) Schematic of the considered plate-like metastructure and photo of the specimen, reproduced from [89]. (c) Enlarged top and side views of the acoustic

metamaterial sheet and measurements of transmitted noise levels from the inner speaker generating 630–1250 Hz noise inside the boxes with and without the acoustic metamaterial sheets, reproduced from [90]. (d) Unit cell of the realizable locally resonant metamaterials plate and the KU Leuven Soundbox clamped with the LRM plate and clamped onto the front wall transmission opening reproduced from [91]. (e) Pictures and schematic of the three types of small-scale resonator and the tested panel configurations with resonators, reproduced from [92].

3.2.2. Cantilever Beam Type Local Resonance Plate-Type Metamaterial

The oscillator in a typical local resonance plate-type metamaterial introduced above needs two materials to act as the mass and spring structures. Cantilever beam oscillators are widely used and can be made of a single material. As shown in Figure 6d, Van Belle et al. studied the sound insulation performance of infinite and finite local resonance plate-type metamaterials with cantilever beams. By introducing the equivalent plate method based on dispersion curves, predictions based on dispersion curves were able to be extended to approximate predictions of the STL. At the same time, insertion loss measurements of an effective area of A2 size (420 × 594 mm) containing 532 resonator specimens were taken through a KU Leuven Soundbox. The study showed that in the infinite periodic structure, the inclusion of damping can improve the accuracy of sound insulation performance predictions [91]. Droz et al. studied the cantilever beam local oscillator at three frequencies considering different additional masses by three laying methods on aircraft-reinforced curved panel skin, as shown in Figure 6e. The sound insulation performance was tested in a reverberation chamber and an anechoic chamber. The results showed that the use of multi-frequency resonance can expand the sound insulation bandwidth. At the same time, by superimposing a melamine foam layer with a thickness of 50.8 mm, it was shown that the narrowband effects of the resonator and the broadband effect of the foam were almost a superposition of the respective STL advantages [92]. A multi-resonant cantilever beam metamaterial plate will be introduced later [93].

3.2.3. Other Types and Multiple Resonance of Local Resonant Plate-Type Metamaterial

As shown in Figure 7a, Ang et al. studied a plate-type acoustic metamaterial with an internal sound cavity resonator by investigating the effect of the shape and depth of the resonator's small orifice on damping and through impedance tube tests and FEM predictions. The results showed that the resonator effect was suppressed by the viscous boundary layer formed along the hole neck. Either the hole neck length (or partition wall thickness) can be reduced, or larger holes can be used [94]. Ang et al. further proposed another plate-type acoustic metamaterial with an internal acoustic cavity resonator, as shown in Figure 7b. A comparative study was conducted on the impact of the presence of a resonator and the arrangement of the resonators on the plate. The sound insulation of a specimen with a size of 994 mm × 994 mm was measured between two reverberation chambers. The results showed that the structure had a better broadband sound insulation performance at 125–400 Hz and 0.8–5 kHz, and the large-size design was not sensitive to the direction and arrangement of the local cavity [95]. Under lightweight and broadband sound insulation consideration, Xi et al. proposed an inertial amplification (IA) acoustic metamaterial (AMM) plate. As shown in Figure 7c, the structure amplified many small particles periodically distributed in its unit cell. The sound pressure level radiated by the specimen was measured in an anechoic chamber using a soundproof cover. The results showed that the STL of the structure was significant, and systematic improvements were achieved over a wide frequency range of 116–544 Hz [96]. Zhang et al. proposed a perforated plate acoustic metamaterial (PAM), as shown in Figure 7d. Based on the electroacoustic analogy, an acoustic impedance analysis of the perforated metamaterial was performed. Through finite element and impedance tube sound insulation studies, the results showed that PAMs can produce good broadband STL at relatively low frequencies. Finally, the designed perforated PAM was applied to the compressor compartment of a commercial refrigerator. The test results verified that the structure satisfied both noise

reduction and ventilation requirements [97]. Other sound transmission and attenuation research on novel structures includes coiled-up spatial metamaterials [98] and origami-based acoustic metamaterials [99].

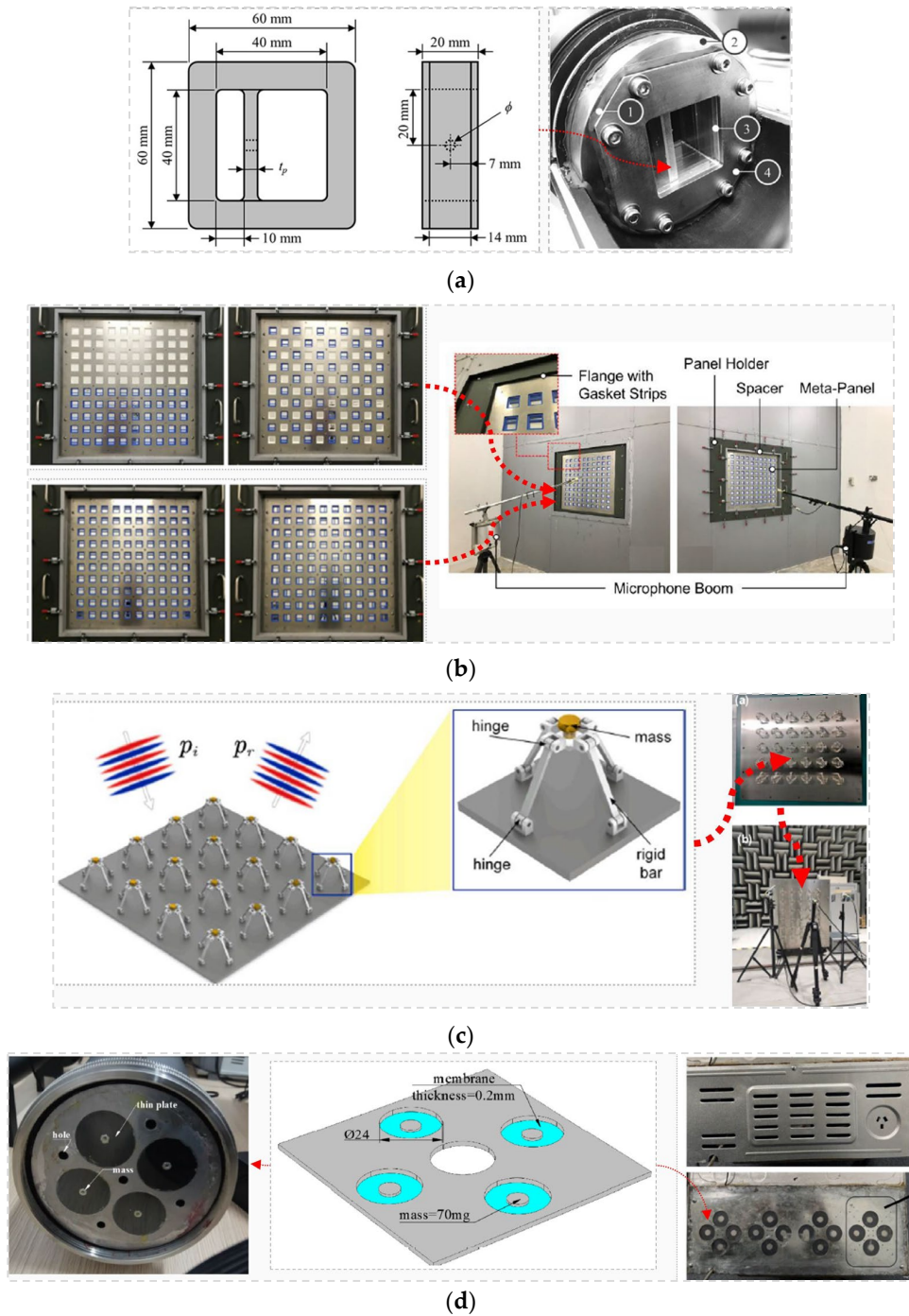


Figure 7. Other types of local resonance plate-type metamaterial. (a) Schematic representation of the specimen viewed from the front and the side and overview of the holder and the specimen mounted in the impedance tube, reproduced from [94]. (b) Setup of the different aluminum meta-panels and the setup for measuring sound pressure levels, reproduced from [95]. (c) Schematic of plane wave transmission through and close view of one single unit cell taken from the inertia amplification acoustic metamaterial plate, reproduced from [96]. (d) Test setup and specimen of the plate-type acoustic metamaterial and the back cover of the compressor compartment of a refrigerator with and without a perforated cover, reproduced from [97].

To broaden the sound insulation frequency band, dual-frequency and multi-frequency local resonance structures have been proposed. As shown in Figure 8a, de Melo Filho et al. aimed to attenuate the first-order acoustic modal response of the cavity structure, proposing to combine two differently tuned local resonant components in the same metamaterial panel to achieve multiple stopbands. The insertion loss of a thermoformed panel of size A2 (420 mm × 594 mm) was tested in a KU Leuven Soundbox. The results showed that the proposed thermoformed metamaterial panel had a similar weight to the original panel but achieved superior insertion loss in the stopband frequency range. The sound pressure level corresponding to the frequency of the first acoustic mode inside the cavity achieved an 8 dB peak reduction [100]. Langfeldt et al. researched the bandwidth improvement of plate-type acoustic metamaterials (PAMs) by using multiple masses or multilayers of PAMs stacked on each other in a unit cell, as shown in Figure 8b, using the modal parameters of the PAM unit cell and the transfer matrix method to predict the single layer and multilayer PAM STL. A large sample structure with a size of 1 m × 1.2 m, containing 180 cylindrical units, was tested between a reverberation chamber and a semi-anechoic chamber. The results showed that at 220 Hz and below, the test values were greater than the simulation results of the infinite period boundary, and other mid- and high-frequency infinite simulation results were in good agreement with the results of the finite test structure. Based on the particle swarm optimization algorithm, the sound insulation bandwidth of the structure between 100 and 400 Hz was optimized when taking the mass into consideration [63]. Zhou et al., by attaching multiple layers of paired rubber and metal cylinders to a thin plate, as shown in Figure 8c, showed that multiple bending wave band gaps in the low-frequency range could be obtained [61]. Dong et al. proposed a metamaterial plate with a double-mass membrane-type resonator (DMMR), as shown in Figure 8d. Combining polynomial fitting and virtual spring methods, the natural frequency characteristics of the resonator and the characteristics of the metamaterial plate were obtained, which showed multiple band gaps [101]. Li et al. proposed an acoustic metamaterial structure with a four-vibrator phononic crystal, as shown in Figure 8e. The semi-analytical method combined with finite element analysis was used to predict the sound insulation, and the single-cell crystal was tested through a square impedance tube. Finally, a cylindrical sleeve structure was designed for a rolling rotor compressor [102].

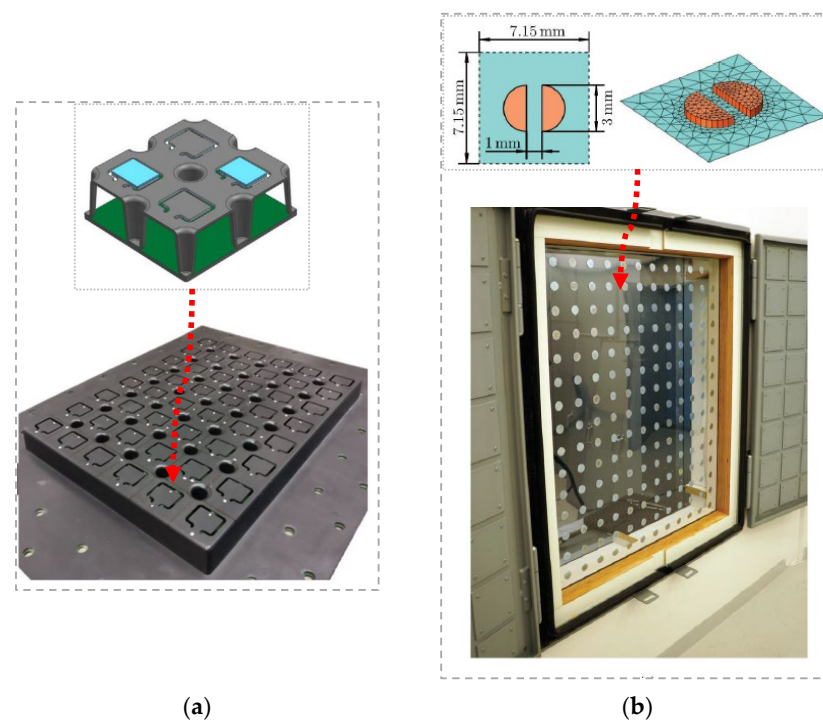


Figure 8. Cont.

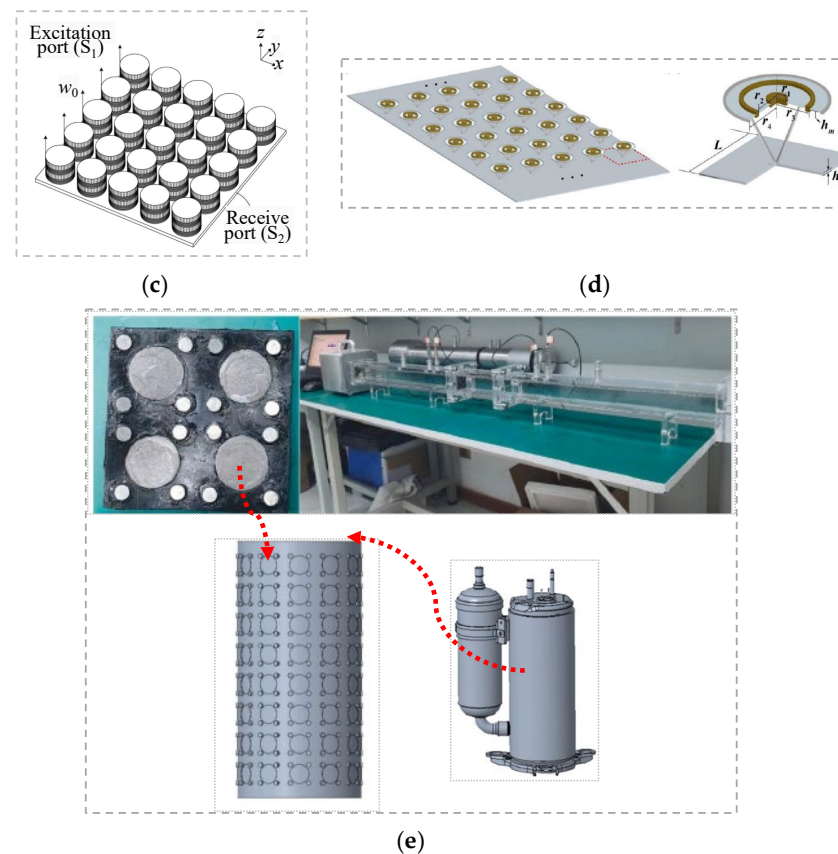


Figure 8. Multiple resonance frequencies plate-type metamaterial. (a) The mixed configuration unit cell and the photo of the thermoformed panel metamaterial, reproduced from [100]. (b) Unit cell geometry, mesh, and the diffuse sound transmission loss test sample measured, reproduced from [63]. (c) Schematic illustration of the calculation of flexural wave transmission, reproduced from [61]. (d) Infinite and unit cell of the metamaterial plate diagram, reproduced from [101]. (e) Four vibrators, acoustic metamaterial samples, sound insulation testing arrangement, and the assembly model, reproduced from [102].

3.2.4. Effects of Boundaries and Temperature

In addition to focusing on the design of the plate-type metamaterial structure itself, scholars have also discussed and studied factors such as boundaries and temperature in practical engineering applications. Considering the influence of non-rigid boundaries of the unit cell, as shown in Figure 9a, Langfeldt et al. studied the influence of non-rigid boundaries of membrane-type and plate-type acoustic metamaterials. A method based on a grid of Euler–Bernoulli beams was developed to model the elastic unit cell edges, and their vibration modes and STL were predicted. The results showed that even if the unit cell edges are not assumed to be fixed, the membrane-type and plate-type acoustic metamaterials can still effectively reduce low-frequency noise [62]. Considering boundary-constrained displacement discontinuity, as shown in Figure 9b, a semi-analytical method was proposed to analyze the vibration of a local resonance plate structure with discontinuous thickness and displacement. It was shown that by applying free boundary conditions to the resonator, the low-order local vibration frequencies could be significantly reduced by up to 90%, while the effect on the low-order global frequencies was negligible [103]. The effect of temperature on the band gap, as shown in Figure 9c, was studied theoretically and through finite element numerical simulation. The temperature change formula and effective mass of the one-dimensional spring mass metamaterial dispersion characteristics were derived. The vibration attenuation characteristics and directional transmission characteristics were studied, and it was found that the elastic wave field can be manipulated through tempera-

ture [104]. In some noise control situations, both ventilation and noise reduction need to be considered. Peng et al. proposed a novel acoustic metamaterial of air-permeable multiple-parallel-connection folding chambers and achieved a balance between sound insulation and ventilation [105]. Trematerra et al. studied three-dimensional metamaterials that can both realize ventilation and sound insulation for air mechanical ventilation systems [106] based on the authors' previous research on acoustic barriers [107,108]. Other research also includes the response of acoustic metamaterials under fluid excitation [109,110] and nonlinear band gaps [111,112].

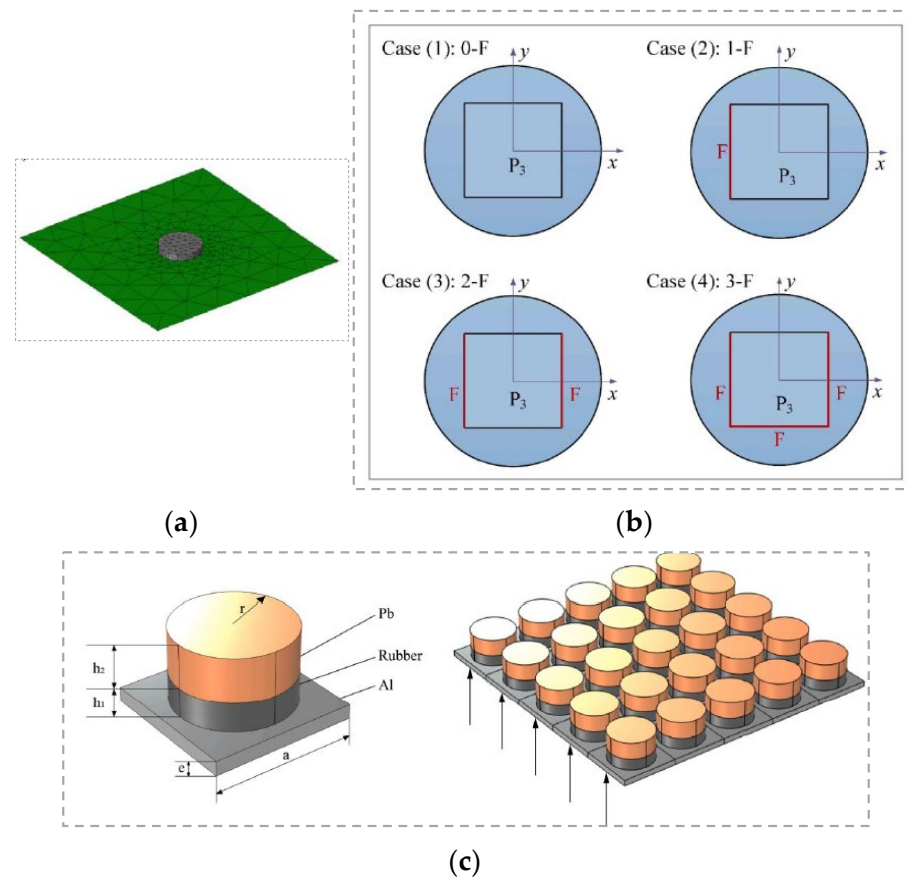


Figure 9. Boundaries and temperature research related to plate-type metamaterial. (a) Computational mesh for the metamaterial unit cell, reproduced from [62]. (b) Schematic diagram of thin plate type resonators with four boundary configurations, reproduced from [103]. (c) Schematic unit-cell of metastructure and the boundary harmonic loading direction of 5×5 finite structure, reproduced from [104].

3.3. Smart Metamaterials for Sound Insulation

Smart metamaterials, also known as active piezoelectric acoustic metamaterials, provide or output electrical energy to achieve energy exchange with sound waves. Piezoelectric materials generate electric charges when the structure deforms when external load is applied. The inverse piezoelectric effect is the mechanical response of the structure when an external electric field is applied [26,113]. The main advantage of piezoelectric smart metamaterials is that the sound insulation frequency band only needs to be adjusted by the external circuit without modifying the metamaterial structure [26].

3.3.1. Classic Piezoelectric Plate-Type Metamaterial

A typical piezoelectric sound insulation metamaterial is created by periodically affixing piezoelectric material sheets to a substrate. As shown in Figure 10a, Zhang et al. studied shunted piezoelectric patch plate-type sound insulation metamaterials and developed an

effective medium method to calculate their sound insulation. The results showed that shunt piezoelectric patches can achieve higher STL within the mass law and coincident region than cases without shunts [114]. Zhang et al. further studied the ultra-thin aluminum foil smart metamaterial structure bonded to piezoelectric resonators, as shown in Figure 10b. The sound insulation performance of a single-cell specimen with a fixed, rigid boundary ($60\text{ mm} \times 60\text{ mm}$) was measured using an impedance tube to verify the simulation model. Numerical and experimental results showed that the metamaterial could break the traditional sound insulation mass law by 30 dB at low frequencies ($<1000\text{ Hz}$), with an ultra-light areal mass density ($<1.6\text{ kg/m}^2$) and ultra-thin structural thickness [68]. Zhang et al. tested the sound insulation of large tunable metamaterial panel samples with a relatively large size of $0.5\text{ m} \times 0.5\text{ m}$ and 36 (6×6) unit cells through a sound attenuator, as shown in Figure 10c to examine the effective dynamic adjustability of the mass density and sound insulation properties [115]. Ji et al. measured the circuit adjustability of the sound transmission performance of piezoelectric metamaterials, as shown in Figure 10d, and established a general analysis model to derive the acoustic properties of piezoelectric acoustic metamaterials through the equivalent transmission matrix method for normal incident waves. The results showed that the sound resonant frequency and bandwidth can be controlled over a wide range of propagation using only external circuit parameters. Layered piezoelectric Ams exhibit excellent performance in terms of tunability and compactness for space-sensitive applications and have great potential in combining metamaterials with electronic control [116].

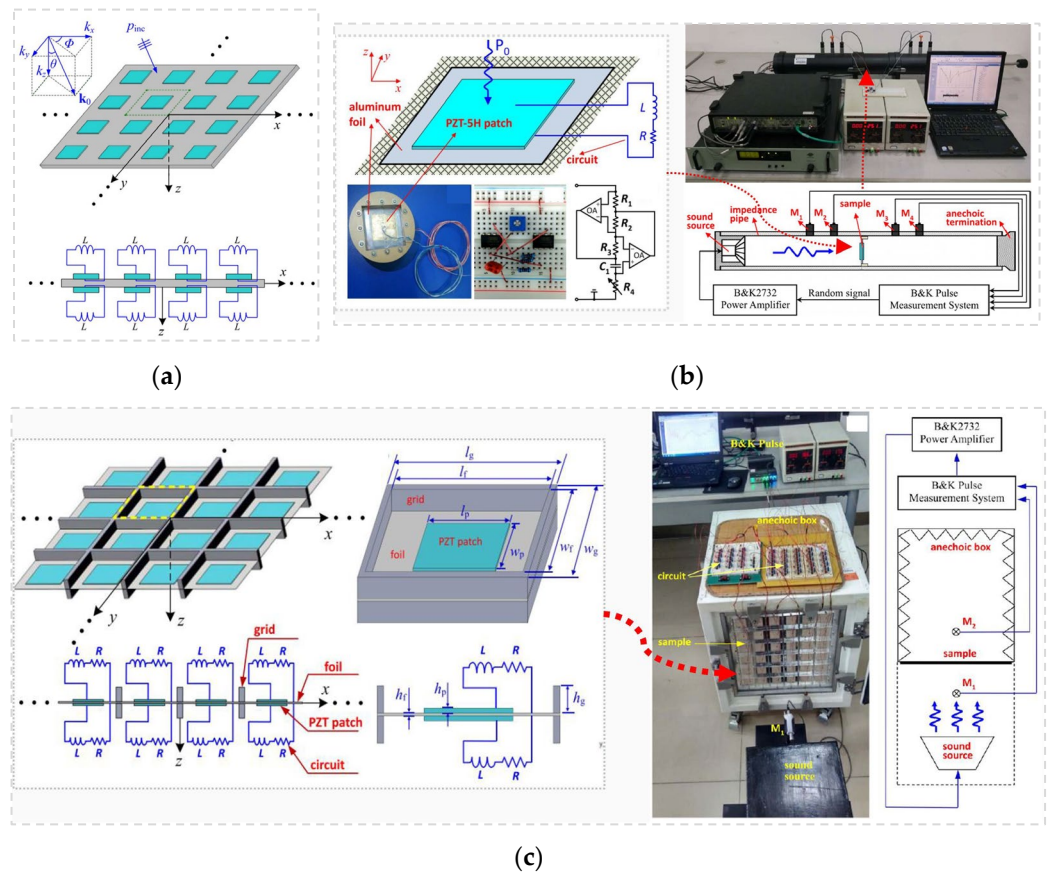


Figure 10. Cont.

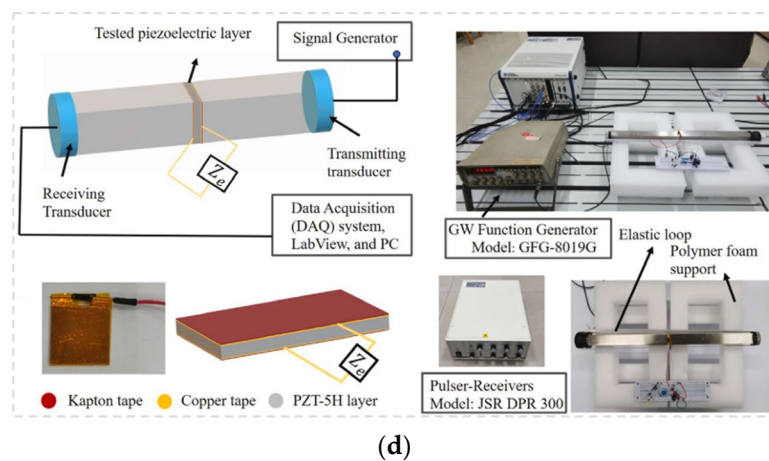


Figure 10. Classic piezoelectric plate-type metamaterial. (a) Schematic diagram and side view of the metamaterial thin plate with periodic arrays of shunted piezoelectric patches, reproduced from [114]. (b) Sketch of the smart acoustic metasurface, photo, and sketch of the experimental setup, reproduced from [68]. (c) Sketch of the tunable acoustic metamaterial panel, photo, and sketch of the experimental setup, reproduced from [115]. (d) Schematic test facility, fabricated piezoelectric layer, and supporting structures, reproduced from [116].

3.3.2. More Complex Piezoelectric Plate-Type Metamaterials

As shown in Figure 11a, Gao et al. designed a new perforated metamaterial plate composed of acoustic black holes (ABHs) interconnected with piezoelectric studs. Based on the differential quadrature element method and first-order shear deformation plate theory, the governing equations of the metamaterial plate were derived, and the results showed that the structure can manipulate bending waves to achieve broadband vibration absorption and directional wave propagation [117]. Schmidt et al. studied the vibroacoustic performance of gradient piezoelectric metamaterial plates, as shown in Figure 11b, through the electromechanical coupling of metamaterial plates. Gradients were achieved in the electrical domain through independent tuning of the resonant frequency of each unit. The effects of linearly varying gradients on vibration attenuation, sound power, kinetic energy, and sound radiation efficiency were studied. Gradient metamaterial plates outperformed their periodic local resonance counterparts in terms of vibration and radiated sound power attenuation [118]. He et al. proposed a metamaterial with active feedback-controlled elastic wave orthogonal stiffeners under external mean flow excitation, as shown in Figure 11c. The effective density was obtained through the effective medium method. Based on the Bloch–Floquet theorem and Poisson’s summations, the spatial harmonic expansion method of the virtual work principle was applied to STL. The effective mass density exhibited frequency-dependent characteristics, and the effective parameters and sound transmission of the structure could be adjusted through active feedback control and acceleration and displacement feedback control actions [119].

Soft active materials (soft elastomers, dielectric elastomers, and magneto-active elastomers), as large deformation response materials, can also actively tune the band gaps and expand the band gap tunability [120]. Most of the studies research the wave and band gap tunable property, which is seldom expanded to sound insulation. For example, Padmanabhan et al. recently presented a theoretical model to obtain the significant tunability of the bandgap in the two-phase hard magnetic soft composite structures when subjected to proper magnetic flux density direction [120].

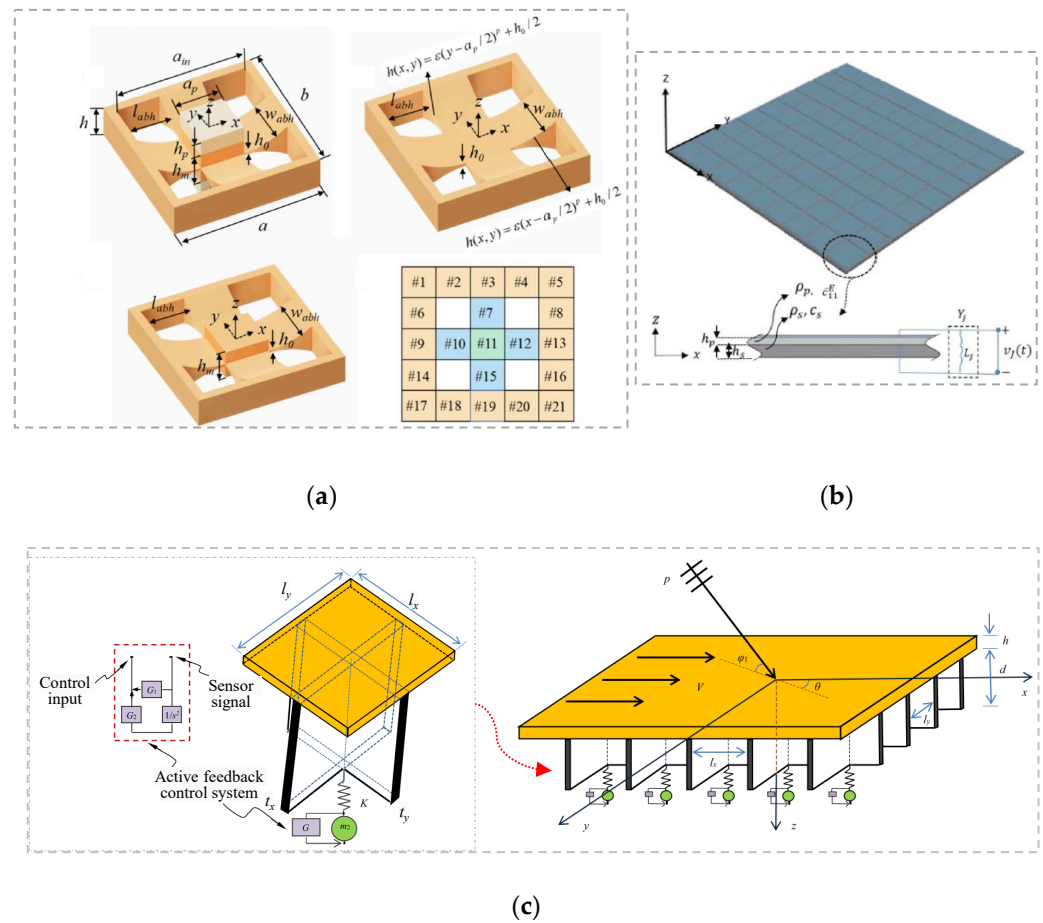


Figure 11. More complex piezoelectric plate-type metamaterials. (a) Schematic of different type unit cells and the decomposition of the unit cell for the proposed metamaterial plates, reproduced from [117]. (b) Schematic of metastructure with piezoelectric layer, reproduced from [118]. (c) Unit cell of the elastic wave metamaterial and the elastic wave metamaterial with the external mean flow, reproduced from [119].

3.4. Composite Sound Insulation Structure Combined with Metamaterials

Some research has focused on the use of metamaterial structures combined with other panel structures, such as the combination of sandwich structure and plate-type metamaterials, the combination of double-panel cavity structures and Helmholtz resonators, etc. Therefore, this section introduces the composite panel sound insulation structure based on the metamaterial structure.

As shown in Figure 12a, Song et al. studied the impact of boundary conditions, namely supported and clamped, on sound insulation and found that the stopband concept of sandwich panels combined with periodic local resonance structures can improve sound insulation over a wider frequency band. At the same time, attention should be paid to the impact of boundary adjustment on the stop band [121].

To break through the mass law, many composite structures, such as panel cavity structures, have been designed to improve sound insulation by introducing cavity layers. While the mass–cavity–mass characteristic frequency f_{MAM} between the plates and cavities inevitably appears, the sound insulation valley value of f_{MAM} is problematic, and this frequency is usually a low frequency [49]. Therefore, to improve this and improve the sound insulation valley value of f_{MAM} , some scholars have introduced metamaterial local oscillators into the plate cavity structure.

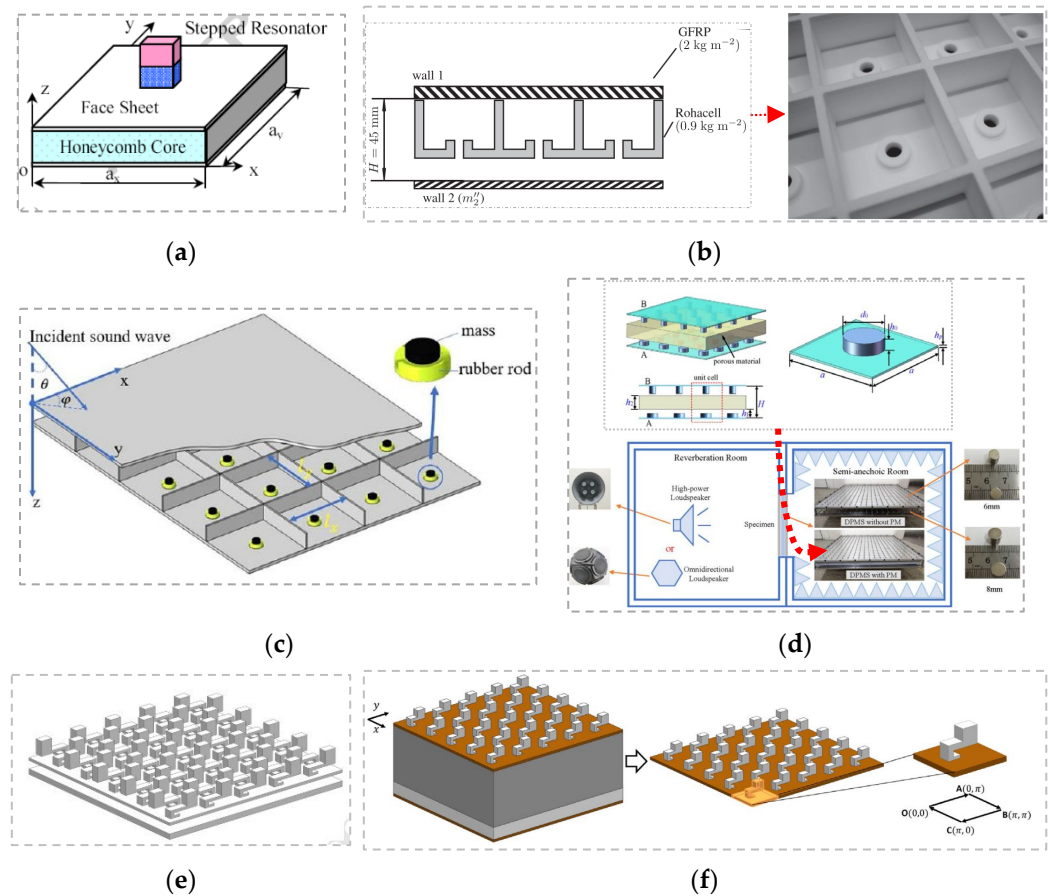


Figure 12. Improvement of f_{MAM} composite sound insulation metamaterials. (a) Sound transmission model of the finite resonant sandwich plate, reproduced from [121]. (b) Structure of the double wall with active Helmholtz resonators test samples and photograph of the Helmholtz resonator panel used in the experiments, reproduced from [122]. (c) Description of an acoustic metamaterial sandwich pane, reproduced from [123]. (d) Unit cell and schematic of a double-panel metastructure lined with porous material and schematic of experimental environment for measurement STL, reproduced from [124]. (e) Schematic of the metamaterial configuration, reproduced from [125]. (f) Complete metamaterial double panel, periodic structure analysis, and corresponding unit cell, reproduced from [126].

3.4.1. Composite Metamaterials Related to the Improvement of f_{MAM}

As shown in Figure 12b, Langfeldt et al. proposed an analytical model to describe the vibroacoustic behavior of a double-layer wall with a Helmholtz resonator, and they verified the feasibility of the model through actual measurements. A double-plate acoustic metamaterial structure of $1\text{ m} \times 1.2\text{ m}$ containing 252 Helmholtz resonator arrays was tested based on the sound insulation of the reverberation chamber and semi-anechoic chamber. The embedded Helmholtz resonator changed the effective bulk modulus of the air cavity and improved the STL at the mass–air–mass resonant frequency [122]. Wang et al. designed a new acoustic metamaterial sandwich panel with enhanced STL by periodically distributing local resonators in the reinforced core, as shown in Figure 12c. The effective dynamic mass density method, the spatial harmonic expansion method, and the principle of virtual work were used. The sound insulation of a sample with a diameter of 99 mm was tested using an impedance tube. Experimental and theoretical results showed that the STL curve had a peak close to the target frequency of the local resonator, which improved the sound insulation properties at frequencies near the mass–air–mass resonance [123]. Wang et al. proposed a double-panel metamaterial with broadband low-frequency sound insulation, which consisted of two layers of metamaterial plates lined with porous material,

as shown in Figure 12d. A semi-analytical method based on the transfer matrix method was proposed and verified by testing large samples (800 mm × 800 mm) using a reverberation chamber and a semi-anechoic chamber [124]. de Melo Filho et al. introduced a local resonance structure on one panel of the double-plate cavity structure, conducted STL prediction based on the dynamic mass method, and measured the sound insulation performance of a sample (420 mm × 591 mm) by the KU Leuven Soundbox small cabin, as shown in Figure 12e. The results showed that under the same mass, after using the local resonance vibration acoustic metamaterial, the sound insulation performance of the double panel structure at f_{MAM} was improved [125]. Styrofoam layers were further introduced into the locally resonant double-plate cavity structure, as shown in Figure 12f. The resonant metamaterial with locally reactive core material demonstrated its potential to improve STL in the f_{MAM} region. The insulation loss, also measured with the KU Leuven Soundbox, was significantly improved [126].

3.4.2. More Complex Large Size Multi-Layer Acoustic Metamaterial

In addition to the above structures that improve sound insulation at f_{MAM} frequencies of double-plate cavity structures, more complex multi-layer acoustic metamaterial structures are introduced here, most of which have also been studied in sound insulation tests on large-size specimens. Varanasi et al. designed a combination of metamaterial panels with waveguide structures and sound-absorbing materials, as shown in Figure 13a. By embedding the metamaterial layer at the transmitting end between the normalized waveguide layer and the absorption layer on the incident side, a hybrid barrier system was formed. The STL of a 1.2 m square panel system consisting of 18×18 square unit cells was tested based on the sound intensity method in a reverberant and semi-anechoic chamber. The hybrid barrier system was found to be the most mass-efficient sound barrier compared to conventional solutions, especially at low frequencies [127]. Wang et al. proposed a new type of plate resonator metamaterial sandwich plate, consisting of a bolts and nuts composition, as shown in Figure 13b. The band gap characteristics of the metamaterial sandwich plate containing a two-dimensional periodic array of plate resonators were numerically modeled by finite element methods, the structural energy band and transmission spectrum were obtained, and a metamaterial sandwich plate specimen was produced and subjected to vibration excitation tests to verify the simulation model, which verified the effective reduction of vibration transmission by the metamaterial structure [128]. In order to adjust and improve the low-frequency sound insulation performance of traditional sandwich structures, Lin et al. proposed a complex resonant acoustic metamaterial composite sandwich structure, as shown in Figure 13c, which was composed of a top panel with a hole at the center, an upper stiffener, a middle thin plate with a cylindrical mass, a lower stiffener, and a bottom pane. An analytical model was established to evaluate its STL, validated through measurement of a standard reverberation chamber with a sample size of 1142 mm × 1142 mm, consisting of 1024 (32×32) unit cells. The analysis results showed that the sound insulation performance in the low frequency range was better than that of orthogonal rib-reinforced sandwich structures themselves and the perforated or plate-type acoustic rib-reinforced sandwich structure metamaterial [129]. Gu et al. designed a multi-layer plate type sandwiched with porous materials, as shown in Figure 13d, which consisted of five layers: three layers of constrained plate-type acoustic metamaterials (denoted as CAM-1, CAM-2, and CAM-3) sandwiched with two layers of porous material (denoted PM-1 and PM-2). The finite element method and measurement through an acoustic impedance tube, along with the reverberant sound insulation of large-scale samples (11×9 unit cells per piece), showed that the larger the sample size, the closer the STL results were to those of a single unit cell with Floquet–Bloch boundary conditions. The laminate acoustic metamaterial (LPAM) composed of multi-layer acoustic metamaterials sandwiched with porous materials effectively isolated broadband low-frequency noise [130]. Yang et al. proposed a multi-layer coupled plate acoustic metamaterial (MPAM) consisting of a metamaterial plate unit, a high-density layer (FB1), and a low-density layer (FB2). The acoustic metamaterial (PAM)

consisted of layers of fibers, as shown in Figure 13e. The insertion loss of the structure was predicted based on FEM. The sound insulation of a sample with a size of 506 mm × 506 mm, composed of 64 periodic square metamaterial units, was tested in a reverberation-anechoic chamber. The results showed that in the range of 360~500 Hz, the IL increased by at least 5 dB, with a maximum increase of up to 17 dB [131].

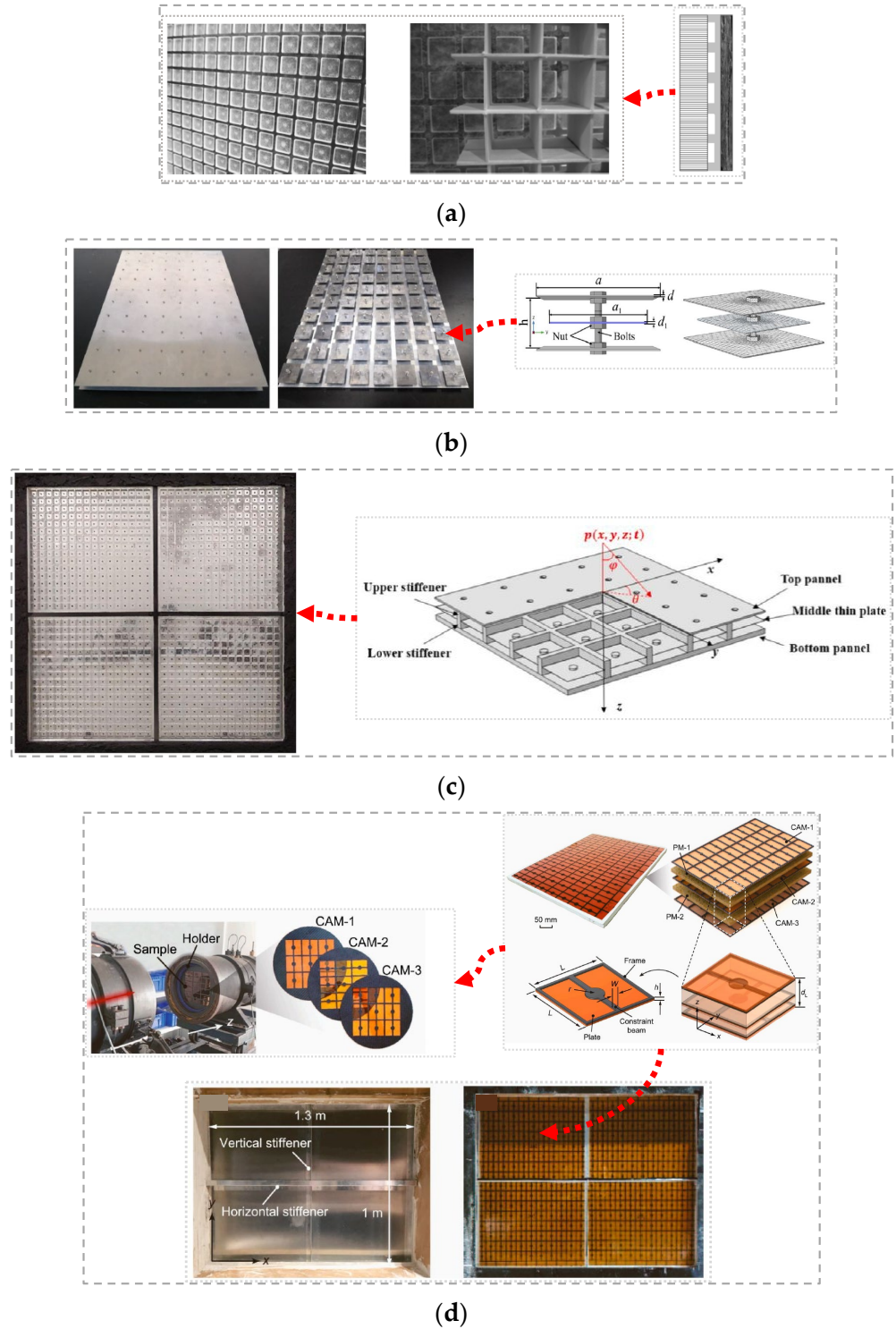


Figure 13. Cont.

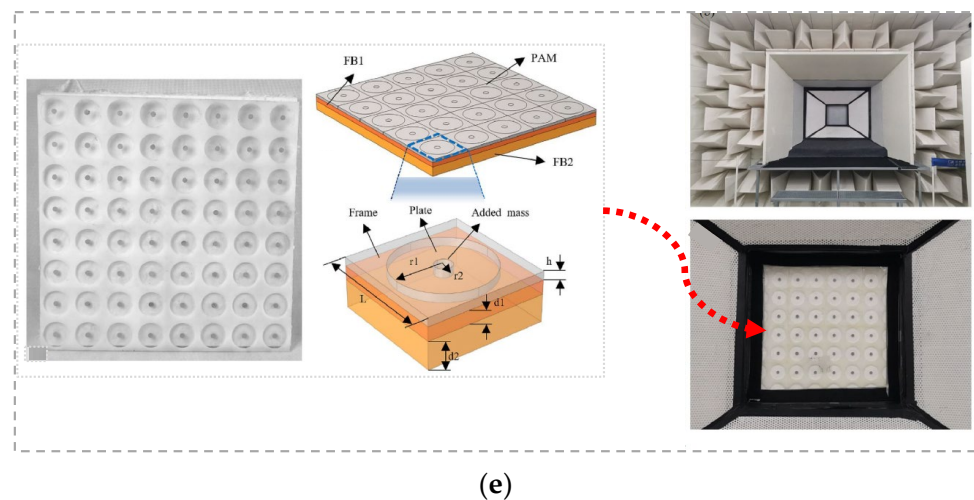


Figure 13. More complex composite sound insulation metamaterials. (a) Hybrid metamaterial panel and its photographs of assembly of sound normalizing layer, cellular panel, and sound absorbing layer, reproduced from [127]. (b) Unit cell of the metamaterial sandwich plate, meshing, and photos of the experimental specimen, reproduced from [128]. (c) Schematic diagram of sandwich structure compounded with resonant acoustic metamaterial and the photograph of the sample, reproduced from [129]. (d) Unit cell and photographs of small- and large-scale experimental samples and setup for the STL measurements, reproduced from [130]. (e) Photos and schematic diagram of typical multilayer coupled plate-type acoustic metamaterials sample, periodic unit, and test site diagrams, reproduced from [131].

3.4.3. Other Novel Combination Metamaterials

In addition to the above multi-layer sound insulation structures incorporating metamaterials, other novel combination structures have also been developed. Li et al. designed a sandwich structure in combination with a membrane and Helmholtz resonator, as shown in Figure 14a, which combined the acoustic advantages of membrane-type acoustic metamaterials and the sandwich structure. The resonant frequency and out-of-plane displacement of membrane-type acoustic metamaterials have been derived and calculated. The sound insulation performance was obtained through FEM modeling, and a sample with a diameter of 100 mm was tested through an impedance tube to verify the accuracy of the model. Research showed that the average sound insulation of the new sandwich structure in the 50~1600 Hz frequency band was 30% higher than that of the single-membrane sandwich structure, and as the boundary constraints were enhanced, the natural frequency of the structure became larger, and the corresponding STL also increased [132]. Jang et al. developed a synergistic sound insulation acoustic metamaterial (SSAM) composed of a membrane and a local resonance structure (LRS), as shown in Figure 14b. The dynamic effective density estimated by the impedance model illustrated the sound insulation mechanism of the design, and its sound insulation performance was verified by finite element modeling simulation. The radiated sound pressure of the sample under acoustic excitation was measured in a semi-anechoic chamber, verifying its excellent low-frequency and broadband sound insulation effects [133]. To avoid a sharp absorption peak that cannot achieve critical coupling in the rectangular sonic black hole at low frequencies, Hruška et al. designed the slits of the rectangular sonic black hole to be partially filled with porous materials, as shown in Figure 14c. The porous material fills the outline of the slit and is superimposed on the sonic black hole profile itself, achieving a significant improvement in the absorption coefficient. The sound absorption coefficient of the structure was measured through an impedance tube [134]. Other novel sound-absorbing metamaterials can achieve high sound-absorption performance at medium and low frequencies [135–137].

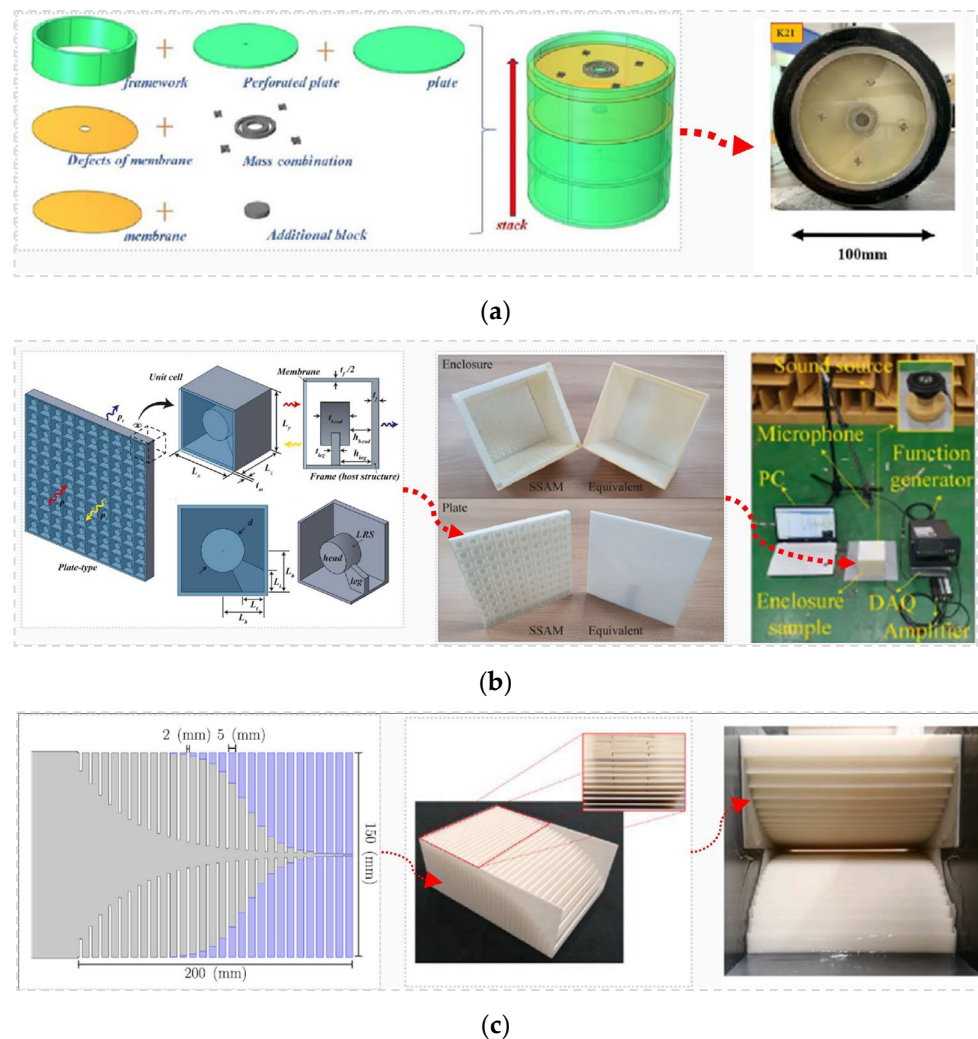


Figure 14. Other novel combinations of metamaterials. (a) Design element and sample of sandwich structure of double membrane-type acoustic metamaterials combined with a Helmholtz resonator structure placed in the impedance tube, reproduced from [132]. (b) Illustration of the synergetic soundproofing acoustic metamaterial plate, its unit cell, and picture of sound pressure level experimental setup, reproduced from [133]. (c) Geometry of the studied sonic black hole with partial porous filling (marked in blue), reproduced from [134].

3.5. Optimization

Optimization is a design method to improve sound insulation, and the optimization of traditional sound insulation wall panels [71,73,74,138–143], as well as metamaterial topology optimization [144], has received increasing attention. Similarly, researchers have combined optimization methods with fixed structures to optimize the sound insulation performance in the frequency band of interest for membrane-type metamaterials. Peng et al., based on the Kriging surrogate model and non-dominated sorting method, optimized the low-frequency sound insulation design of membrane-type acoustic metamaterials, as shown in Figure 15a. The results showed that when multi-parameter coupling is performed, the influence of a single variable on the sound insulation peak remains unchanged; however, the degree of impact is different [145]. Peng et al. presented an optimization that considered both fatigue and lightweight sound absorption, as shown in Figure 15b. To ensure the low-frequency sound absorption performance while achieving a lightweight design, a multi-objective particle swarm optimization algorithm was used. The results showed that with the proposed lightweight method, the corresponding minimum fatigue life was increased by 10.27%. In addition, the impedance tube test results showed that the average

sound absorption coefficient of the optimized structure increased by 41.6% compared with that before optimization. The total weight of the optimized structure was 25.9% lighter [146].

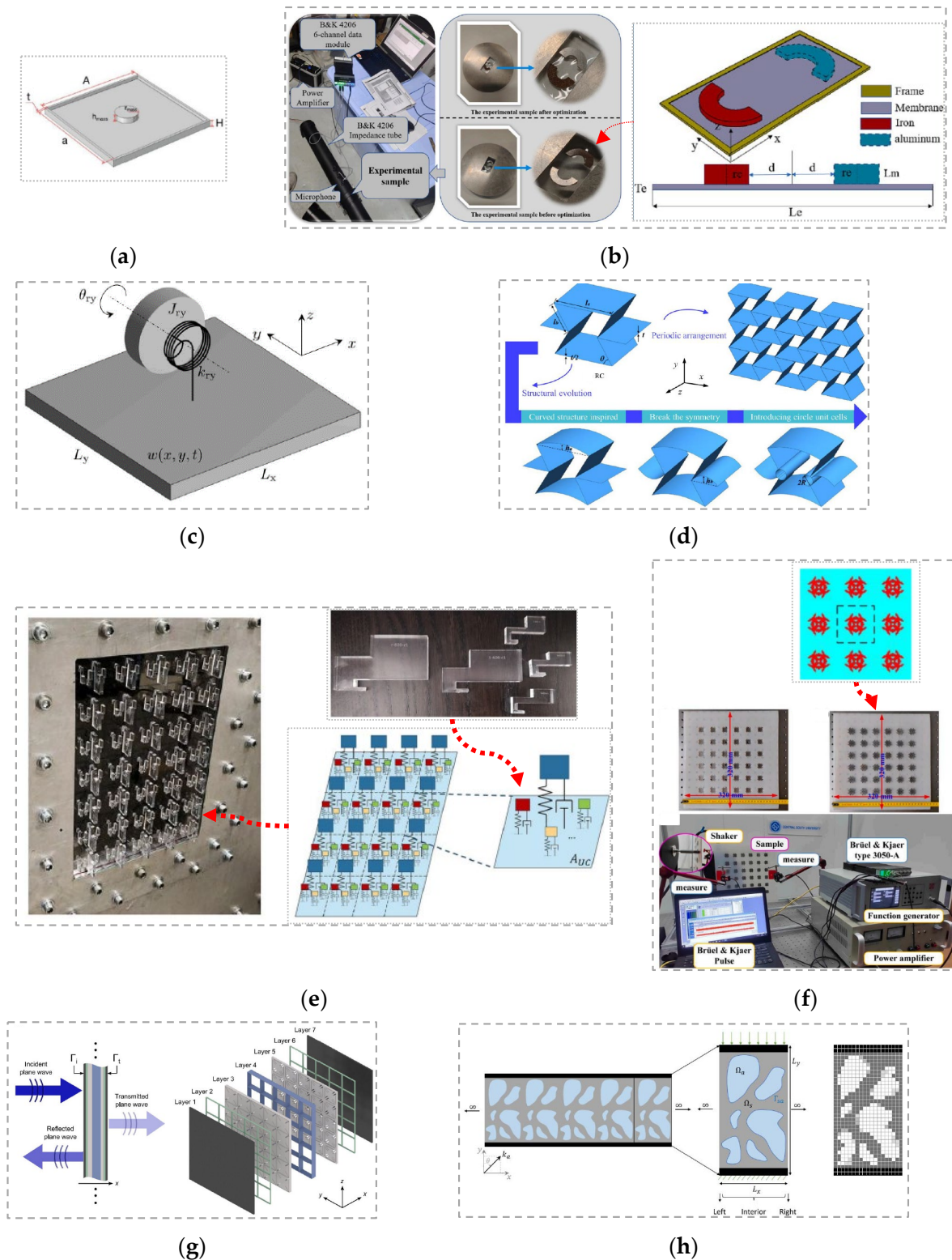


Figure 15. Metamaterial STL optimization. (a) Schematic of the structure, reproduced from [145]. (b) Proposed structure for lightweight optimization and schematic diagram of the experimental

setup and the experimental samples of the proposed structure, reproduced from [146]. (c) Scheme of the locally resonant metamaterials unit cell with attached single degree of freedom rotational resonators, reproduced from [147]. (d) Schematic diagram and structural evolutionary route of re-entrant cellular metamaterials, reproduced from [148]. (e) Photos of STL measurement setup and illustration of the unit cell and finite periodic metamaterial panel with idealized mass–spring–damper resonators, reproduced from [93]. (f) Fabricated samples for thin elastic metamaterial plates composed of the optimized unit cells arranged on the 6×6 square lattice, reproduced from [149]. (g) Sound transmission loss evaluation setup and representation of the multi-resonant layered acoustic metamaterials layered structure, reproduced from [150]. (h) Supercell considered in the numerical model where the green indications symbolize the force and boundary condition used in the computation of the stiffness constraint, and the example of the structured FE discretization, reproduced from [151].

Optimization of the sound insulation or band gap of some plate-type metamaterials has been a focus of research [63]. For the orthotropic base plate structure, as shown in Figure 15c, Giannini et al. proposed an orthotropic metamaterial with rotating resonators that exhibits direction dependence, as well as combining translational and rotational modes, making it effective over a wide frequency band. An effective analytical medium theoretical model was developed, and a genetic algorithm was used to optimize the sound insulation performance [147]. Han et al. used reinforcement learning to optimize the structural parameters of honeycomb metamaterials, as shown in Figure 15d, to obtain the maximum band gap [148]. Janssen et al. designed a multi-resonant cantilever beam metamaterial plate, as shown in Figure 15e. A sound insulation prediction model through the finite element, combined with MATLAB, was used to optimize the mass–spring resonator structure, and finally, an A3 size specimen was tested in a reverberation chamber. It was shown that the STL was improved compared with traditional metamaterial panels [93]. Yan et al. predicted the band gap characteristics of structures based on the improved fast plane wave expansion method, combined with an adaptive genetic algorithm, to achieve the topology optimization of different shapes and spatial distributions of materials in a unit cell. Under excitation, the vibration transmissibility of the optimized 6×6 unit cell metamaterial thin plate sample was measured, as shown in Figure 15f. The results showed that out-of-plane bending waves can be transmitted or blocked [149]. Zhang et al. optimized the lightweight average sound insulation of local resonant panels in the center frequency band of 20~800 Hz. Under lightweight optimization, the resonator improved the sound insulation effect in the local frequency bands. It was also found that the average broadband sound insulation can approach but not exceed the average sound insulation provided by bare boards of equal mass [58].

For multi-layer sound insulation structures that introduce metamaterials, scholars have also considered sound insulation optimization. Sal-Anglada et al. developed a novel computational design strategy to optimize the STL performance of metamaterials and optimize multi-resonant layered acoustic metamaterials, as shown in Figure 15g, through a homogenization method [150]. Cool et al. combined the noise and vibration suppression properties of metamaterials with sandwich panels and the potential of lightweight load-bearing structures to propose a topology optimization framework for the vibroacoustic design of core materials in sandwich structures, as shown in Figure 15h. This limited the volume and structural stiffness while minimizing sound transmission. The effectiveness of the model was verified through FEM, and the design was lightweight, load-bearing, and achieved high sound insulation in the frequency band from 1000 Hz to 3000 Hz, exceeding the mass law by 15–40 dB [151]. There are many studies on the band gap and other characteristics of topology-optimized acoustic metamaterials [152,153], but less research on sound insulation based on topology optimization.

4. Discussion

4.1. Fabrication Approaches Statistic

Fabrication is a key bridge between applications and AM structural design. Liao et al. divided approaches into three typical categories, namely, conventional fabrication approaches, additive manufacturing approaches, and miscellaneous fabrication approaches [1]. Table 1 gives the fabrication approach statistics of STL metamaterial test samples. Among them, 3D printing is relatively more used, and there are also mechanical processing and direct use of magnets and metal plates as metamaterials. However, due to the complexity of internal coiled-up space, many small support structures are inevitably added to the interior of the sample during the 3D printing process, which could be one of the reasons for the discrepancy [98]. This is also a challenge faced by all 3D/4D printing metamaterials, namely high-precision 3D printing technology of multiple materials [67].

Table 1. Fabrication approaches statistics of STL metamaterial test samples.

	Metamaterial	Impedance Tube Test	Acoustic Room Test
Related research	membrane-type	[60,77,83,85–88,146]	[76,82]
	plate-type	[94,97,102]	[63,89,92,95,96]
	composite	[98,99,122,132,134]	[122,124,127,129–131,133]
Statistics of fabrication approaches	<ul style="list-style-type: none"> • membrane-type, hyper elastic material + supporting or starching structure: [82,87,88,146]. • magnets as a mass block: [87,89,124]. • machining: [94,122,127]. • 3D printing: [83,92,95,98,133,134]. • combine the lathe machining and 3D printing: [132]. 		

A membrane-type metamaterial can obtain tension through the difference in thermal expansion coefficient between the membrane and support [86]. Support structures or stretching mechanisms are also used, but the uniform inner-stress distribution was a great challenge for a tensioned membrane [88].

4.2. Challenges

Through the classification introduction and manufacturing method statistics of the above sound-insulating metamaterials, Table 2 compares and discusses the sound-insulating metamaterials in terms of frequency STL and its challenges. Although the membrane-type and plate-type sound insulation metamaterials have complex structures, their sound insulation peaks are fixed after the structure is finalized, and the peak frequency band is limited and relatively narrow. At the same time, the membrane structure's lifespan, stability, uniform inner-stress distribution, etc., need to be broken through. The sound insulation peak of intelligent metamaterials is adjustable, but it depends on external equipment and maintenance. The composite structure can improve the sound insulation from a wider frequency band, and the selection of its composite structure combination and the parameter design that considers it lightweight is worth extensive and in-depth research.

Table 2. STL Performance and challenges of metamaterials.

Metamaterial	STL Performance	Challenges
Membrane-type	fixed and narrow frequency range	fragile, and uniform inner-stress distribution was a challenge
Plate-type	fixed and narrow frequency range	complex geometry, manufacturing cost
Smart	tunable frequency range	external wiring or other maintenance
Composite	wide frequency range	appropriate combination selection, complex models, large number of design parameters, large amount of calculation, etc.

5. Conclusions and Outlook

This work reviewed the research progress of sound insulation metamaterials in recent years, discussing different design structures, research methods, research results, etc. In general, the research on the sound insulation of thin-walled metamaterials has made great progress:

- STL prediction research methods are becoming increasingly abundant, from finite element simulations to theoretical methods, semi-analytical methods, etc.;
- Measurement now ranges from impedance tube testing of single-cell structures to large-scale multi-cell structures;
- The design of metamaterial cells has expanded from a single frequency to multiple frequencies, including passive and active metamaterials;
- The research covers metamaterial structures to composite panel structures based on metamaterial structures, such as composite multi-layer structures containing metamaterials that are combined with plate cavities and sound-absorbing materials, etc.;
- The parameter investigation to optimize the lightweight sound insulation metamaterial design has been covered, considering the frequency band sound insulation performance.

Although the above results have been achieved, the research on sound insulation metamaterial structures still needs to be improved. The existing research mainly focuses on theory, simulation, and laboratory testing, with fewer papers considering the implementation of sound insulation in actual engineering applications. Sound insulation devices in engineering usually have relatively large areas. This is a restriction of additive manufacturing for relatively complex structures with metamaterials. For example, plate AM is difficult to achieve due to its complex structure and relatively small single-cell band gap. Therefore, it has higher process requirements and challenges for materials, structures, precision, etc. On the other hand, it has more stringent requirements for the materials themselves. For example, film-type AM has a short lifespan, easily undergoes deformation, and has an unstable performance, all of which need to be overcome. The development of 3D/4D printing technology is a potential solution, but the high-precision 3D printing technology of multiple materials needs to be improved.

The application of multi-objective optimization can promote the development of high-performance sound insulation metamaterials, especially when the sound insulation structure needs to consider factors such as lightweight, cost, frequency sound insulation performance, and the overall sound insulation performance (R_w or averaged STL single evaluator of wide frequency band). It is worth noting that there are many studies on the band gap and other characteristics of topology-optimized acoustic metamaterials but less research on the sound insulation based on topology optimization. Topology optimization targeting sound insulation has its theoretical basis and prospects.

There are few studies on sound insulation metamaterial structures that simultaneously consider dimensions, boundary conditions, temperature, excitation characteristics (turbulence, sound waves), and other factors. As the above review results, both boundary and temperature et al. will have an influence on the effect of the AM. For existing materials and manufacturing processes, if the above factors can be considered based on actual application scenarios, combined with the sound insulation advantages of various composite plate structures, with the appropriate sound insulation evaluation indicators selected and optimized, lightweight sound insulation structures may be obtained. This may be one way to further promote the engineering applications and development of sound insulation metamaterial structures. For vehicles such as aircraft and cars, the research and application of composite sound insulation metamaterials containing damping and sound absorbing materials on the fuselage or body is expected to improve the acoustic performance (especially at low frequency) in the cabin or car. Of course, the insulation performance of metamaterial can be more effective if the factors mentioned above can be considered.

Expanding the high sound insulation frequency band of metamaterials has always been the pursuit of researchers. Combining the advantages of various composite panel structures with optimization methods and a proper wide frequency band single evaluator

has the potential to improve the sound insulation performance of composite metamaterials in the full frequency range. The detailed study of the different combinations and sound insulation mechanisms will also contribute to the engineering application of metamaterials.

This paper mainly concentrates on the sound insulation AM; the detailed development and properties of sound absorption and vibration isolation AMs will also be focused on in the future.

6. Patents

There are no patents resulting from the work reported in this manuscript.

Author Contributions: Conceptualization, Y.Z. (Yumei Zhang) and J.Z.; writing—original draft preparation, Y.Z. (Yumei Zhang), Y.L. and D.Y.; writing—review and editing, J.Z. and Y.Z. (Yue Zhao); visualization, Y.A., W.P. and J.L. All authors have read and agreed to the published version of the manuscript.

Funding: This research was funded by the National Key R&D Program of China (No. 2021YFF0603904), the National Nature Science Foundation of China (62203451), the Natural Science Foundation of Sichuan Province of China (2022NSFSC1897, 2023JDRC0004, 2023NSFSC0902), the Open Project of Key Laboratory of Flight Techniques and Flight Safety, CAAC (No. FZ2022KF01), and by the Fundamental Research Funds for the Central Universities (PHD2023-044, PHD2023-009).

Conflicts of Interest: The authors declare no conflict of interest.

References

- Liao, G.; Luan, C.; Wang, Z.; Liu, J.; Yao, X.; Fu, J. Acoustic Metamaterials: A Review of Theories, Structures, Fabrication Approaches, and Applications. *Adv. Mater. Technol.* **2021**, *6*, 2000787. [[CrossRef](#)]
- Veselago, V.G. Electrodynamics of substances with simultaneously negative electrical and magnetic permeabilities. *Soviet Physics Uspekhi* **1968**, *10*, 504–509. [[CrossRef](#)]
- Sim, J.; Zhao, R.R. Magneto-Mechanical Metamaterials: A Perspective. *J. Appl. Mech.* **2024**, *91*, 031004. [[CrossRef](#)]
- Pendry, J.B. Negative refraction makes a perfect lens. *Phys. Rev. Lett.* **2000**, *85*, 3966–3969. [[CrossRef](#)] [[PubMed](#)]
- Chen, M.; Wang, C.; Cheng, X.; Gong, C.; Song, W.; Yuan, X.; Fang, D. Experimental demonstration of invisible electromagnetic impedance matching cylindrical transformation optics cloak shell. *J. Opt.* **2018**, *20*, 045608. [[CrossRef](#)]
- Prakash, D.; Gupta, N. Applications of metamaterial sensors: A review. *Int. J. Microw. Wirel. Technol.* **2021**, *14*, 19–33. [[CrossRef](#)]
- Sigalas, M.M. Elastic and acoustic wave band structure. *J. Sound Vib.* **1992**, *158*, 377–382. [[CrossRef](#)]
- Kushwaha, M.S.; Halevi, P.; Dobrzynski, L.; Djafari-Rouhani, B. Acoustic band structure of periodic elastic composites. *Phys. Rev. Lett.* **1993**, *71*, 2022–2025. [[CrossRef](#)]
- Sánchez-Pérez, J.V.; Caballero, D.; Martínez-Sala, R.; Rubio, C.; Sánchez-Dehesa, J.; Meseguer, F.; Llinares, J.; Gálvez, F. Sound Attenuation by a Two-Dimensional Array of Rigid Cylinders. *Phys. Rev. Lett.* **1998**, *80*, 5325–5328. [[CrossRef](#)]
- Liu, Z.; Zhang, X.; Mao, Y.; Zhu, Y.Y.; Yang, Z.; Chan, C.T.; Sheng, P. Locally resonant sonic materials. *Science* **2000**, *289*, 1734–1736. [[CrossRef](#)]
- Liu, Z.; Chan, C.T.; Sheng, P. Three-component elastic wave band-gap material. *Phys. Rev. B* **2002**, *65*, 165116. [[CrossRef](#)]
- Ciaburro, G.; Iannace, G. Membrane-type acoustic metamaterial using cork sheets and attached masses based on reused materials. *Appl. Acoust.* **2022**, *189*, 108605. [[CrossRef](#)]
- Ciaburro, G.; Parente, R.; Iannace, G.; Puyana-Romero, V. Design Optimization of Three-Layered Metamaterial Acoustic Absorbers Based on PVC Reused Membrane and Metal Washers. *Sustainability* **2022**, *14*, 4218. [[CrossRef](#)]
- Qiu, C.; Zhang, X.; Liu, Z. Far-field imaging of acoustic waves by a two-dimensional sonic crystal. *Phys. Rev. B* **2005**, *71*, 054302. [[CrossRef](#)]
- Zhao, Y.; Dong, H.Y.; Zhao, S.; Min, S.; Cheng, J.; Li, B.; Chi, F.; Liu, S. Design of broadband impedance-matching Bessel lens with acoustic metamaterials. *J. Appl. Phys.* **2019**, *126*, 065103. [[CrossRef](#)]
- Tang, H.; Hao, Z.; Zang, J. Nonplanar acoustic metasurface for focusing. *J. Appl. Phys.* **2019**, *125*, 154901. [[CrossRef](#)]
- Chen, Y.; Liu, X.; Hu, G. Influences of imperfectness and inner constraints on an acoustic cloak with unideal pentamode materials. *J. Sound Vib.* **2019**, *458*, 62–73. [[CrossRef](#)]
- Cummer, S.A.; Christensen, J.; Alù, A. Controlling sound with acoustic metamaterials. *Nat. Rev. Mater.* **2016**, *1*, 16001. [[CrossRef](#)]
- Huang, T.Y.; Shen, C.; Jing, Y. Membrane- and plate-type acoustic metamaterials. *J. Acoust. Soc. Am.* **2016**, *139*, 3240–3250. [[CrossRef](#)]
- Chen, S.; Fan, Y.; Fu, Q.; Wu, H.; Jin, Y.; Zheng, J.; Zhang, F. A Review of Tunable Acoustic Metamaterials. *Appl. Sci.* **2018**, *8*, 1480. [[CrossRef](#)]
- Ma, F.; Wang, C.; Liu, C.; Wu, J.H. Structural designs, principles, and applications of thin-walled membrane and plate-type acoustic/elastic metamaterials. *J. Appl. Phys.* **2021**, *129*, 231103. [[CrossRef](#)]

22. Tao, Y.; Ren, M.; Zhang, H.; Peijs, T. Recent progress in acoustic materials and noise control strategies—A review. *Appl. Mater. Today* **2021**, *24*, 101141. [[CrossRef](#)]
23. Zarastvand, M.R.; Ghassabi, M.; Talebitooti, R. Prediction of acoustic wave transmission features of the multilayered plate constructions: A review. *J. Sandw. Struct. Mater.* **2021**, *24*, 218–293. [[CrossRef](#)]
24. Gao, N.; Zhang, Z.; Deng, J.; Guo, X.; Cheng, B.; Hou, H. Acoustic Metamaterials for Noise Reduction: A Review. *Adv. Mater. Technol.* **2022**, *7*, 2100698. [[CrossRef](#)]
25. Gibson, B.; Nguyen, T.; Sinaie, S.; Heath, D.; Ngo, T. The low frequency structure-borne sound problem in multi-storey timber buildings and potential of acoustic metamaterials: A review. *Build. Environ.* **2022**, *224*, 109531. [[CrossRef](#)]
26. Ji, G.; Huber, J. Recent progress in acoustic metamaterials and active piezoelectric acoustic metamaterials—A review. *Appl. Mater. Today* **2022**, *26*, 101260. [[CrossRef](#)]
27. Zhang, L.; Sheng, X. A review on the research progress of mechanical meta-structures and their applications in rail transit. *Intell. Transp. Infrastruct.* **2022**, *1*, liac010. [[CrossRef](#)]
28. Yin, J.; Cai, L.; Fang, X.; Xiao, Y.; Yang, H.; Zhang, H.; Zhong, J.; Zhao, H.; Yu, D.; Wen, J. Review on research progress of mechanical metamaterials and their applications on vibration and noise control. *Adv. Mech.* **2022**, *52*, 508–586. [[CrossRef](#)]
29. Liu, D.; Hao, L.; Zhu, W.; Yang, X.; Yan, X.; Guan, C.; Xie, Y.; Pang, S.; Chen, Z. Recent Progress in Resonant Acoustic Metasurfaces. *Materials* **2023**, *16*, 7044. [[CrossRef](#)]
30. Zhang, J.; Hu, B.; Wang, S. Review and perspective on acoustic metamaterials: From fundamentals to applications. *Appl. Phys. Lett.* **2023**, *123*, 010502. [[CrossRef](#)]
31. Xiao, Y.; Wang, Y.; Zhao, H.; Yu, D.; Wen, J. Research Progress of Acoustic Metamaterials for Vibration and Noise Reduction Applications. *J. Mech. Eng.* **2023**, *59*, 277–298.
32. Thompson, D. *Railway Noise and Vibration: Mechanisms, Modelling and Means of Control*; Elsevier: Amsterdam, The Netherlands, 2008.
33. Zhang, J.; Xiao, X.; Sheng, X.; Zhang, C.; Wang, R.; Jin, X. SEA and contribution analysis for interior noise of a high speed train. *Appl. Acoust.* **2016**, *112*, 158–170. [[CrossRef](#)]
34. Zhang, Y.; Thompson, D.; Squicciarini, G.; Ryue, J.; Xiao, X.; Wen, Z. Sound transmission loss properties of truss core extruded panels. *Appl. Acoust.* **2018**, *131*, 134–153. [[CrossRef](#)]
35. Lee, H.P.; Kumar, S.; Garg, S.; Lim, K.M. Assessment of in-cabin noise of wide-body aircrafts. *Appl. Acoust.* **2022**, *194*, 108809. [[CrossRef](#)] [[PubMed](#)]
36. Bertsch, L.; Simons, D.G.; Snellen, M. *Aircraft Noise-The Major Sources, Modelling Capabilities, and Reduction Possibilities*; DLR: Göttingen, Germany, 2015.
37. Ballesteros, J.A.; Sarradj, E.; Fernández, M.D.; Geyer, T.; Ballesteros, M.J. Noise source identification with Beamforming in the pass-by of a car. *Appl. Acoust.* **2015**, *93*, 106–119. [[CrossRef](#)]
38. Zhang, J.; Xiao, X.; Wang, D.; Yang, Y.; Fan, J. Source Contribution Analysis for Exterior Noise of a High-Speed Train: Experiments and Simulations. *Shock Vib.* **2018**, *2018*, 5319460. [[CrossRef](#)]
39. Petrone, G.; Melillo, G.; Laudiero, A.; De Rosa, S. A Statistical Energy Analysis (SEA) model of a fuselage section for the prediction of the internal Sound Pressure Level (SPL) at cruise flight conditions. *Aerosp. Sci. Technol.* **2019**, *88*, 340–349. [[CrossRef](#)]
40. Hopkins, C. *Sound Insulation*; Routledge: London, UK, 2012.
41. Fahy, F.; Thompson, D. *Fundamentals of Sound and Vibration*; CRC Press: Boca Raton, FL, USA, 2015.
42. Mulholland, K.A.; Parbrook, H.D.; Cummings, A. The transmission loss of double panels. *J. Sound Vib.* **1967**, *6*, 324–334. [[CrossRef](#)]
43. Au, A.C.K.; Byrne, K.P. On the insertion losses produced by plane acoustic lagging structures. *J. Acoust. Soc. Am.* **1987**, *82*, 1325–1333. [[CrossRef](#)]
44. London, A. Transmission of reverberant sound through single walls. *J. Res. Natl. Bur. Stand.* **1949**, *42*, 605–615. [[CrossRef](#)]
45. Xie, G.; Thompson, D.J.; Jones, C.J.C. A modelling approach for the vibroacoustic behaviour of aluminium extrusions used in railway vehicles. *J. Sound Vib.* **2006**, *293*, 921–932. [[CrossRef](#)]
46. Langley, R.S.; Cotoni, V. Response variance prediction for uncertain vibro-acoustic systems using a hybrid deterministic-statistical method. *J. Acoust. Soc. Am.* **2007**, *122*, 3445–3463. [[CrossRef](#)] [[PubMed](#)]
47. Langley, R.S.; Bremner, P. A hybrid method for the vibration analysis of complex structural-acoustic systems. *J. Acoust. Soc. Am.* **1999**, *105*, 1657–1671. [[CrossRef](#)]
48. Nilsson, C.; Thite, A.; Jones, C.; Thompson, D.J. Estimation of sound transmission through extruded panels using a coupled waveguide finite element-boundary element method. In Proceedings of the Noise and Vibration Mitigation for Rail Transportation Systems: Proceedings of the 9th International Workshop on Railway Noise, Munich, Germany, 4–8 September 2007; Springer: Berlin/Heidelberg, Germany, 2008; pp. 306–312.
49. Lu, T.; Xin, F. *Vibro-Acoustics of Lightweight Sandwich Structures*; Springer: Berlin/Heidelberg, Germany, 2014.
50. Cremer, L.; Heckl, M. *Structure-Borne Sound: Structural Vibrations and Sound Radiation at Audio Frequencies*; Springer Science & Business Media: Berlin/Heidelberg, Germany, 2013.
51. Santoni, A.; Davy, J.L.; Fausti, P.; Bonfiglio, P. A review of the different approaches to predict the sound transmission loss of building partitions. *Build. Acoust.* **2020**, *27*, 253–279. [[CrossRef](#)]
52. Chen, Y.; Huang, G.; Zhou, X.; Hu, G.; Sun, C.T. Analytical coupled vibroacoustic modeling of membrane-type acoustic metamaterials: Membrane model. *J. Acoust. Soc. Am.* **2014**, *136*, 969–979. [[CrossRef](#)]

53. Cheng, Y.; Zhou, C.; Yuan, B.G.; Wu, D.J.; Wei, Q.; Liu, X.J. Ultra-sparse metasurface for high reflection of low-frequency sound based on artificial Mie resonances. *Nat. Mater.* **2015**, *14*, 1013–1019. [[CrossRef](#)] [[PubMed](#)]
54. Fokin, V.; Ambati, M.; Sun, C.; Zhang, X. Method for retrieving effective properties of locally resonant acoustic metamaterials. *Phys. Rev. B* **2007**, *76*, 144302. [[CrossRef](#)]
55. Li, Y.; Liang, B.; Gu, Z.M.; Zou, X.Y.; Cheng, J.C. Reflected wavefront manipulation based on ultrathin planar acoustic metasurfaces. *Sci. Rep.* **2013**, *3*, 2546. [[CrossRef](#)]
56. Li, Y.; Jiang, X.; Li, R.-q.; Liang, B.; Zou, X.-y.; Yin, L.-l.; Cheng, J.-c. Experimental Realization of Full Control of Reflected Waves with Subwavelength Acoustic Metasurfaces. *Phys. Rev. Appl.* **2014**, *2*, 064002. [[CrossRef](#)]
57. Xiao, Y.; Wen, J.; Wen, X. Sound transmission loss of metamaterial-based thin plates with multiple subwavelength arrays of attached resonators. *J. Sound Vib.* **2012**, *331*, 5408–5423. [[CrossRef](#)]
58. Zhang, Y.; Li, Y.; Zhao, Y.; Yao, D.; Ai, Y.; Pan, W. Lightweight sound insulation optimization of simply supported locally resonant plate. *J. Vib. Control* **2023**. [[CrossRef](#)]
59. Bortot, E.; Amir, O.; Shmuel, G. Topology optimization of dielectric elastomers for wide tunable band gaps. *Int. J. Solids Struct.* **2018**, *143*, 262–273. [[CrossRef](#)]
60. Wang, X.; Zhao, H.; Luo, X.; Huang, Z. Membrane-constrained acoustic metamaterials for low frequency sound insulation. *Appl. Phys. Lett.* **2016**, *108*, 041905. [[CrossRef](#)]
61. Zhou, X.; Wang, L.; Qin, L.; Peng, F. Improving sound insulation in low frequencies by multiple band-gaps in plate-type acoustic metamaterials. *J. Phys. Chem. Solids* **2020**, *146*, 109606. [[CrossRef](#)]
62. Langfeldt, F.; Gleine, W. Membrane- and plate-type acoustic metamaterials with elastic unit cell edges. *J. Sound Vib.* **2019**, *453*, 65–86. [[CrossRef](#)]
63. Langfeldt, F.; Gleine, W. Optimizing the bandwidth of plate-type acoustic metamaterials. *J. Acoust. Soc. Am.* **2020**, *148*, 1304–1314. [[CrossRef](#)] [[PubMed](#)]
64. Rayleigh, B. *The Theory of Sound*; Palgrave Macmillan: London, UK, 1896; Volume 3.
65. Yao, D.; Zhang, J.; Wang, R.; Xiao, X. Effects of mounting positions and boundary conditions on the sound transmission loss of panels in a niche. *J. Zhejiang Univ. A* **2020**, *21*, 129–146. [[CrossRef](#)]
66. Wang, R.; Yao, D.; Zhang, J.; Xiao, X.; Li, Y. Effect of installation conditions on laboratory sound insulation measurement and an equivalent method for simply supported boundary. *Appl. Acoust.* **2022**, *188*, 108593. [[CrossRef](#)]
67. Zhou, X.; Ren, L.; Song, Z.; Li, G.; Zhang, J.; Li, B.; Wu, Q.; Li, W.; Ren, L.; Liu, Q. Advances in 3D/4D printing of mechanical metamaterials: From manufacturing to applications. *Compos. Part B Eng.* **2023**, *254*, 110585. [[CrossRef](#)]
68. Zhang, H.; Xiao, Y.; Wen, J.; Yu, D.; Wen, X. Ultra-thin smart acoustic metasurface for low-frequency sound insulation. *Appl. Phys. Lett.* **2016**, *108*, 141902. [[CrossRef](#)]
69. *ISO140-2:1995; Acoustics—Laboratory Measurement of Sound Insulation of Building Elements—Part 2: Measurement of Airborne Sound Insulation*. ISO: Geneva, Switzerland, 1995.
70. *ISO140-3:1995; Acoustics—Measurement of Sound Insulation in Buildings and of Building Elements—Part 3: Laboratory Measurements of Airborne Sound Insulation of Building Elements*. ISO: Geneva, Switzerland, 1995.
71. Yao, D.; Zhang, J.; Wang, R.-Q.; Xiao, X.-B.; Guo, J.-Q. Lightweight design and sound insulation characteristic optimisation of railway floating floor structures. *Appl. Acoust.* **2019**, *156*, 66–77. [[CrossRef](#)]
72. Ou, D.Y. Low frequency sound insulation analysis and evaluation of stiffened building structures. *Build. Environ.* **2015**, *94*, 802–809. [[CrossRef](#)]
73. Li, Y.; Xiao, X.; Zhang, Y.; Tang, Z.; Pan, A. Acoustic optimization design of window of high-speed train under flow-induced vibration. *Appl. Acoust.* **2022**, *201*, 109100. [[CrossRef](#)]
74. Li, Y.; Xiao, X.; Zhang, Y.; Tang, Z.; Pan, A. Acoustic optimization design of porous materials on sandwich panel under flow-induced vibration. *Int. J. Aeroacoust.* **2023**, *22*, 60–84. [[CrossRef](#)]
75. *ISO 717-1:2013; Acoustics—Rating of Sound Insulation in Buildings and of Building Elements—Part 1: Airborne Sound Insulation*. International Organization for Standardization: Geneva, Switzerland, 2013.
76. Hashimoto, N.; Katsura, M.; Yasuoka, M.; Fujii, H. Sound insulation of a rectangular thin membrane with additional weights. *Appl. Acoust.* **1991**, *33*, 21–43. [[CrossRef](#)]
77. Ho, K.M.; Yang, Z.; Zhang, X.X.; Sheng, P. Measurements of sound transmission through panels of locally resonant materials between impedance tubes. *Appl. Acoust.* **2005**, *66*, 751–765. [[CrossRef](#)]
78. Yang, Z.; Mei, J.; Yang, M.; Chan, N.H.; Sheng, P. Membrane-type acoustic metamaterial with negative dynamic mass. *Phys. Rev. Lett.* **2008**, *101*, 204301. [[CrossRef](#)] [[PubMed](#)]
79. Naify, C.J.; Chang, C.-M.; McKnight, G.; Nutt, S. Transmission loss and dynamic response of membrane-type locally resonant acoustic metamaterials. *J. Appl. Phys.* **2010**, *108*, 114905. [[CrossRef](#)]
80. Zhang, Y.; Wen, J.; Xiao, Y.; Wen, X.; Wang, J. Theoretical investigation of the sound attenuation of membrane-type acoustic metamaterials. *Phys. Lett. A* **2012**, *376*, 1489–1494. [[CrossRef](#)]
81. Varanasi, S.; Bolton, J.S.; Siegmund, T.H.; Cipra, R.J. The low frequency performance of metamaterial barriers based on cellular structures. *Appl. Acoust.* **2013**, *74*, 485–495. [[CrossRef](#)]
82. Ang, L.Y.L.; Koh, Y.K.; Lee, H.P. Broadband sound transmission loss of a large-scale membrane-type acoustic metamaterial for low-frequency noise control. *Appl. Phys. Lett.* **2017**, *111*, 041903. [[CrossRef](#)]

83. Cao, E.; Jia, B.; Guo, D.; Li, B.; Wang, W.; Huang, H. Bionic design and numerical studies of spider web-inspired membrane-type acoustic metamaterials. *Compos. Struct.* **2023**, *315*, 117010. [[CrossRef](#)]
84. Li, J.; Jiang, R.; Xu, D.; Huang, Q. Study of acoustic transmission losses in particle-reinforced rubber-based membrane-type acoustic metamaterials. *Appl. Acoust.* **2023**, *208*, 109379. [[CrossRef](#)]
85. Yang, Z.; Dai, H.M.; Chan, N.H.; Ma, G.C.; Sheng, P. Acoustic metamaterial panels for sound attenuation in the 50–1000 Hz regime. *Appl. Phys. Lett.* **2010**, *96*, 041906. [[CrossRef](#)]
86. Naify, C.J.; Chang, C.-M.; McKnight, G.; Nutt, S. Transmission loss of membrane-type acoustic metamaterials with coaxial ring masses. *J. Appl. Phys.* **2011**, *110*, 124903. [[CrossRef](#)]
87. Zhang, Y.; Wen, J.; Zhao, H.; Yu, D.; Cai, L.; Wen, X. Sound insulation property of membrane-type acoustic metamaterials carrying different masses at adjacent cells. *J. Appl. Phys.* **2013**, *114*, 063515. [[CrossRef](#)]
88. Lu, Z.; Yu, X.; Lau, S.-K.; Khoo, B.C.; Cui, F. Membrane-type acoustic metamaterial with eccentric masses for broadband sound isolation. *Appl. Acoust.* **2020**, *157*, 107003. [[CrossRef](#)]
89. Xiao, Y.; Cao, J.; Wang, S.; Guo, J.; Wen, J.; Zhang, H. Sound transmission loss of plate-type metastructures: Semi-analytical modeling, elaborate analysis, and experimental validation. *Mech. Syst. Signal Process.* **2021**, *153*, 107487. [[CrossRef](#)]
90. Nakayama, M.; Matsuoka, T.; Saito, Y.; Uchida, N.; Inoue, K.; Mitani, H.; Akasaka, S.; Koga, S. A practically designed acoustic metamaterial sheet with two-dimensional connection of local resonators for sound insulation applications. *J. Appl. Phys.* **2021**, *129*, 105106. [[CrossRef](#)]
91. Van Belle, L.; Claeys, C.; Deckers, E.; Desmet, W. The impact of damping on the sound transmission loss of locally resonant metamaterial plates. *J. Sound Vib.* **2019**, *461*, 114909. [[CrossRef](#)]
92. Droz, C.; Robin, O.; Ichchou, M.; Atalla, N. Improving sound transmission loss at ring frequency of a curved panel using tunable 3D-printed small-scale resonators. *J. Acoust. Soc. Am.* **2019**, *145*, EL72–EL78. [[CrossRef](#)] [[PubMed](#)]
93. Janssen, S.; Van Belle, L.; de Melo Filho, N.G.R.; Desmet, W.; Claeys, C.; Deckers, E. Improving the noise insulation performance of vibro-acoustic metamaterial panels through multi-resonant design. *Appl. Acoust.* **2023**, *213*, 109622. [[CrossRef](#)]
94. Ang, L.Y.L.; Koh, Y.K.; Lee, H.P. A note on the viscous boundary layer in plate-type acoustic metamaterials with an internal tonraum resonator. *Appl. Acoust.* **2018**, *140*, 160–166. [[CrossRef](#)]
95. Ang, L.Y.L.; Koh, Y.K.; Lee, H.P. Plate-type acoustic metamaterials: Evaluation of a large-scale design adopting modularity for customizable acoustical performance. *Appl. Acoust.* **2019**, *149*, 156–170. [[CrossRef](#)]
96. Xi, C.; Yu, X.; Cheng, L.; Mi, Y. Broadband low-frequency sound insulation of a metamaterial plate with inertial amplification. *Appl. Acoust.* **2023**, *213*, 109655. [[CrossRef](#)]
97. Zhang, Z.; Wang, X.; Liu, Z.Y.; Fan, Q.; Lin, T.R. A study of low frequency sound insulation mechanism of a perforated plate-type acoustic metamaterial. *J. Sound Vib.* **2023**, *558*, 117775. [[CrossRef](#)]
98. Li, Y.; Yan, J. Acoustic transmission characteristics based on coiled-up space metamaterials. *Appl. Acoust.* **2023**, *203*, 109199. [[CrossRef](#)]
99. Wen, G.; Zhang, S.; Wang, H.; Wang, Z.-P.; He, J.; Chen, Z.; Liu, J.; Xie, Y.M. Origami-based acoustic metamaterial for tunable and broadband sound attenuation. *Int. J. Mech. Sci.* **2023**, *239*, 107872. [[CrossRef](#)]
100. de Melo Filho, N.G.R.; Claeys, C.; Deckers, E.; Desmet, W. Realisation of a thermoformed vibro-acoustic metamaterial for increased STL in acoustic resonance driven environments. *Appl. Acoust.* **2019**, *156*, 78–82. [[CrossRef](#)]
101. Dong, W.; Wang, T.; Huang, Z.; Chen, M.; Li, Q.; Jia, W. Characteristics of band gaps of a metamaterial plate with membrane-type resonators based on the energy approach. *Thin-Walled Struct.* **2023**, *191*, 110930. [[CrossRef](#)]
102. Li, J.; Wu, X.; Wang, C.; Huang, Q. Sound insulation prediction and band gap characteristics of four vibrators acoustic metamaterial with composite phononic crystal structure. *Mater. Today Commun.* **2023**, *37*, 107455. [[CrossRef](#)]
103. Xue, J.; Zhang, W.; Wu, J.; Wang, C.; Ma, H. A semi-analytical method for vibration localization of plates integrated with low-frequency plate-type resonators. *Thin-Walled Struct.* **2024**, *194*, 111332. [[CrossRef](#)]
104. Hou, X.; Feng, J.; Yuan, X.; An, X.; Fan, H. Temperature effects on wave attenuation properties of metamaterials: Bandgap drift. *Therm. Sci. Eng. Prog.* **2023**, *39*, 101724. [[CrossRef](#)]
105. Peng, W.; Bi, S.; Shen, X.; Yang, X.; Yang, F.; Wang, E. Study on Sound-Insulation Performance of an Acoustic Metamaterial of Air-Permeable Multiple-Parallel-Connection Folding Chambers by Acoustic Finite Element Simulation. *Materials* **2023**, *16*, 4298. [[CrossRef](#)] [[PubMed](#)]
106. Trematerra, A.; Bevilacqua, A.; Iannace, G. Noise Control in Air Mechanical Ventilation Systems with Three-Dimensional Metamaterials. *Appl. Sci.* **2023**, *13*, 1650. [[CrossRef](#)]
107. Iannace, G.; Berardi, U.; Ciaburro, G.; Trematerra, A. Sound Attenuation of an Acoustic Barrier Made with Metamaterials. *Can. Acoust.* **2019**, *47*, 5–9.
108. Iannace, G.; Ciaburro, G.; Trematerra, A. Metamaterials acoustic barrier. *Appl. Acoust.* **2021**, *181*, 108172. [[CrossRef](#)]
109. Li, Y.; Choy, Y.S. Acoustic behaviour of micro-perforated panel backed by shallow cavity under fully developed grazing flow. *J. Sound Vib.* **2024**, *569*, 117985. [[CrossRef](#)]
110. Schram, C.; Bennett, G.J. Aeroacoustics research in Europe: The CEAS-ASC report on 2022 highlights. *J. Sound Vib.* **2024**, *568*, 117895. [[CrossRef](#)]
111. Shen, Y.; Lacarbonara, W. Nonlinear dispersion properties of metamaterial beams hosting nonlinear resonators and stop band optimization. *Mech. Syst. Signal Process.* **2023**, *187*, 109920. [[CrossRef](#)]

112. Shen, Y.; Lacarbonara, W. Nonlinearity enhanced wave bandgaps in metamaterial honeycombs embedding spider web-like resonators. *J. Sound Vib.* **2023**, *562*, 117821. [[CrossRef](#)]
113. Casadei, F.; Delpero, T.; Bergamini, A.; Ermanni, P.; Ruzzene, M. Piezoelectric resonator arrays for tunable acoustic waveguides and metamaterials. *J. Appl. Phys.* **2012**, *112*, 064902. [[CrossRef](#)]
114. Zhang, H.; Wen, J.; Xiao, Y.; Wang, G.; Wen, X. Sound transmission loss of metamaterial thin plates with periodic subwavelength arrays of shunted piezoelectric patches. *J. Sound Vib.* **2015**, *343*, 104–120. [[CrossRef](#)]
115. Zhang, H.; Chen, S.; Liu, Z.; Song, Y.; Xiao, Y. Light-weight large-scale tunable metamaterial panel for low-frequency sound insulation. *Appl. Phys. Express* **2020**, *13*, 067003. [[CrossRef](#)]
116. Ji, G.; Zhou, J.; Huber, J. The evaluation of electrical circuits for adjusting sound transmission properties of piezoelectric metamaterials. *Mech. Syst. Signal Process.* **2023**, *200*, 110549. [[CrossRef](#)]
117. Gao, W.; Hu, J.; Qin, Z.; Chu, F. Flexural wave manipulation in perforated metamaterial plates with acoustic black holes interconnected by piezoelectric studs. *Compos. Struct.* **2023**, *321*, 117224. [[CrossRef](#)]
118. Schimidt, C.S.; de Oliveira, L.P.R.; De Marqui, C. Vibro-acoustic performance of graded piezoelectric metamaterial plates. *Compos. Struct.* **2024**, *327*, 117656. [[CrossRef](#)]
119. He, Z.-H.; Wang, Y.-Z.; Wang, Y.-S. Sound transmission of active elastic wave metamaterial with double locally resonant substructures surrounded by external mean flow. *Wave Motion* **2023**, *116*, 103088. [[CrossRef](#)]
120. Padmanabhan, S.; Alam, Z.; Sharma, A.K. Tunable anti-plane wave bandgaps in 2D periodic hard-magnetic soft composites. *Int. J. Mech. Sci.* **2024**, *261*, 108686. [[CrossRef](#)]
121. Song, Y.; Feng, L.; Wen, J.; Yu, D.; Wen, X. Reduction of the sound transmission of a periodic sandwich plate using the stop band concept. *Compos. Struct.* **2015**, *128*, 428–436. [[CrossRef](#)]
122. Langfeldt, F.; Hoppen, H.; Gleine, W. Broadband low-frequency sound transmission loss improvement of double walls with Helmholtz resonators. *J. Sound Vib.* **2020**, *476*, 115309. [[CrossRef](#)]
123. Wang, S.; Zhang, X.; Li, F.; Hosseini, S.M. Sound transmission loss of a novel acoustic metamaterial sandwich panel: Theory and experiment. *Appl. Acoust.* **2022**, *199*, 109035. [[CrossRef](#)]
124. Wang, S.; Xiao, Y.; Gu, J.; Hu, C.; Zhang, H.; Wen, J. Double-panel metastructure lined with porous material for broadband low-frequency sound insulation. *Appl. Acoust.* **2023**, *207*, 109332. [[CrossRef](#)]
125. de Melo Filho, N.G.R.; Van Belle, L.; Claeys, C.; Deckers, E.; Desmet, W. Dynamic mass based sound transmission loss prediction of vibro-acoustic metamaterial double panels applied to the mass-air-mass resonance. *J. Sound Vib.* **2019**, *442*, 28–44. [[CrossRef](#)]
126. de Melo Filho, N.G.R.; Claeys, C.; Deckers, E.; Desmet, W. Metamaterial foam core sandwich panel designed to attenuate the mass-spring-mass resonance sound transmission loss dip. *Mech. Syst. Signal Process.* **2020**, *139*, 106624. [[CrossRef](#)]
127. Varanasi, S.; Bolton, J.S.; Siegmund, T. Experiments on the low frequency barrier characteristics of cellular metamaterial panels in a diffuse sound field. *J. Acoust. Soc. Am.* **2017**, *141*, 602–610. [[CrossRef](#)] [[PubMed](#)]
128. Wang, Q.; Li, J.; Zhang, Y.; Xue, Y.; Li, F. Bandgap properties in metamaterial sandwich plate with periodically embedded plate-type resonators. *Mech. Syst. Signal Process.* **2021**, *151*, 107375. [[CrossRef](#)]
129. Lin, Q.; Lin, Q.; Wang, Y.; Di, G. Sound insulation performance of sandwich structure compounded with a resonant acoustic metamaterial. *Compos. Struct.* **2021**, *273*, 114312. [[CrossRef](#)]
130. Gu, J.; Tang, Y.; Wang, X.; Huang, Z. Laminated plate-type acoustic metamaterials with Willis coupling effects for broadband low-frequency sound insulation. *Compos. Struct.* **2022**, *292*, 115689. [[CrossRef](#)]
131. Yang, X.-H.; Kang, Y.; Xie, X.; Zhang, Q.; Shangguan, W.-B. Multilayer coupled plate-type acoustic metamaterials for low-frequency broadband sound insulation. *Appl. Acoust.* **2023**, *209*, 109399. [[CrossRef](#)]
132. Li, H.-Z.; Liu, X.-C.; Liu, Q.; Li, S.; Yang, J.-S.; Tong, L.-L.; Shi, S.-B.; Schmidt, R.; Schröder, K.-U. Sound insulation performance of double membrane-type acoustic metamaterials combined with a Helmholtz resonator. *Appl. Acoust.* **2023**, *205*, 109297. [[CrossRef](#)]
133. Jang, J.-Y.; Song, K. Synergistic acoustic metamaterial for soundproofing: Combining membrane and locally resonant structure. *Int. J. Mech. Sci.* **2023**, *256*, 108500. [[CrossRef](#)]
134. Hruška, V.; Groby, J.-P.; Bednařík, M. Complex frequency analysis and source of losses in rectangular sonic black holes. *J. Sound Vib.* **2024**, *571*, 118107. [[CrossRef](#)]
135. Xu, Q.; Qiao, J.; Sun, J.; Zhang, G.; Li, L. A tunable massless membrane metamaterial for perfect and low-frequency sound absorption. *J. Sound Vib.* **2021**, *493*, 115823. [[CrossRef](#)]
136. Pavan, G.; Singh, S. Near-perfect sound absorptions in low-frequencies by varying compositions of porous labyrinthine acoustic metamaterial. *Appl. Acoust.* **2022**, *198*, 108974. [[CrossRef](#)]
137. Qu, R.; Guo, J.; Fang, Y.; Zhong, S.; Zhang, X. Broadband quasi-perfect sound absorption by a metasurface with coupled resonators at both low- and high-amplitude excitations. *Mech. Syst. Signal Process.* **2023**, *204*, 110782. [[CrossRef](#)]
138. Wang, T.; Li, S.; Nutt, S.R. Optimal design of acoustical sandwich panels with a genetic algorithm. *Appl. Acoust.* **2009**, *70*, 416–425. [[CrossRef](#)]
139. Shojaeifard, M.H.; Talebitooti, R.; Yadollahi, A. Optimization of sound transmission through laminated composite cylindrical shells by using a genetic algorithm. *Mech. Compos. Mater.* **2011**, *47*, 481–494. [[CrossRef](#)]
140. Zhou, J.; Bhaskar, A.; Zhang, X. Bi-objective optimization for the vibro-acoustic performance of a double-wall panel. *J. Acoust. Soc. Am.* **2012**, *131*, 3271. [[CrossRef](#)]

141. Talebitooti, R.; Gohari, H.D.; Zarastvand, M.R. Multi objective optimization of sound transmission across laminated composite cylindrical shell lined with porous core investigating Non-dominated Sorting Genetic Algorithm. *Aerosp. Sci. Technol.* **2017**, *69*, 269–280. [[CrossRef](#)]
142. Talebitooti, R.; Zarastvand, M.; Darvishgohari, H. Multi-objective optimization approach on diffuse sound transmission through poroelastic composite sandwich structure. *J. Sandw. Struct. Mater.* **2021**, *23*, 1221–1252. [[CrossRef](#)]
143. Dal Poggetto, V.F.; Pugno, N.M.; Arruda, J.R.F. Bioinspired periodic panels optimized for acoustic insulation. *Philos. Trans. A Math. Phys. Eng. Sci.* **2022**, *380*, 20210389. [[CrossRef](#)]
144. Li, Z.; Wang, L.; Geng, X.; Chen, W.; Han, B. Complex uncertainty-oriented robust topology optimization for multiple mechanical metamaterials based on double-layer mesh. *Comput. Methods Appl. Mech. Eng.* **2024**, *419*, 116589. [[CrossRef](#)]
145. Peng, W.; Zhang, J.; Shi, M.; Li, J.; Guo, S. Low-frequency sound insulation optimisation design of membrane-type acoustic metamaterials based on Kriging surrogate model. *Mater. Des.* **2023**, *225*, 111491. [[CrossRef](#)]
146. Peng, L.; Bao, B. Optimized membrane-type acoustic metamaterials for alleviating engineering fatigue damage via lightweight optimization. *Eng. Struct.* **2023**, *292*, 116550. [[CrossRef](#)]
147. Giannini, D.; Schevenels, M.; Reynders, E.P.B. Rotational and multimodal local resonators for broadband sound insulation of orthotropic metamaterial plates. *J. Sound Vib.* **2023**, *547*, 117453. [[CrossRef](#)]
148. Han, S.; Han, Q.; Ma, N.; Li, C. Design and reinforcement-learning optimization of re-entrant cellular metamaterials. *Thin-Walled Struct.* **2023**, *191*, 111071. [[CrossRef](#)]
149. Yan, G.; Yao, S.; Li, Y.; Zhou, W. Topological optimization of thin elastic metamaterial plates for ultrawide flexural vibration bandgaps. *Int. J. Mech. Sci.* **2023**, *242*, 108014. [[CrossRef](#)]
150. Sal-Anglada, G.; Yago, D.; Cante, J.; Oliver, J.; Roca, D. Optimal design of Multiresonant Layered Acoustic Metamaterials (MLAM) via a homogenization approach. *Eng. Struct.* **2023**, *293*, 116555. [[CrossRef](#)]
151. Cool, V.; Sigmund, O.; Aage, N.; Naets, F.; Deckers, E. Vibroacoustic topology optimization for sound transmission minimization through sandwich structures. *J. Sound Vib.* **2024**, *568*, 117959. [[CrossRef](#)]
152. Zhang, X.; Xing, J.; Liu, P.; Luo, Y.; Kang, Z. Realization of full and directional band gap design by non-gradient topology optimization in acoustic metamaterials. *Extrem. Mech. Lett.* **2021**, *42*, 101126. [[CrossRef](#)]
153. Sun, P.; Zhang, Z.; Guo, H.; Liu, N.; Jin, W.; Yuan, T.; Wang, Y. Topological optimization of hierarchical honeycomb acoustic metamaterials for low-frequency extreme broad band gaps. *Appl. Acoust.* **2022**, *188*, 108579. [[CrossRef](#)]

Disclaimer/Publisher's Note: The statements, opinions and data contained in all publications are solely those of the individual author(s) and contributor(s) and not of MDPI and/or the editor(s). MDPI and/or the editor(s) disclaim responsibility for any injury to people or property resulting from any ideas, methods, instructions or products referred to in the content.